

INLA-RF: A Hybrid Modeling Strategy for Spatio-Temporal Environmental Data

Mario Figueira^a, Michela Cameletti^{b,*}, Luca Patelli^b

^a*Department of Statistics and Operations Research, University of Valencia, Valencia, Spain*

^b*Department of Economics, University of Bergamo, Bergamo, Italy*

Abstract

Environmental processes often exhibit complex, non-linear patterns and discontinuities across space and time, posing significant challenges for traditional geostatistical modeling approaches. In this paper, we propose a hybrid spatio-temporal modeling framework that combines the interpretability and uncertainty quantification of Bayesian models —estimated using the INLA-SPDE approach— with the predictive power and flexibility of Random Forest (RF). Specifically, we introduce two novel algorithms, collectively named INLA-RF, which integrate a statistical spatio-temporal model with RF in an iterative two-stage framework. The first algorithm (INLA-RF1) incorporates RF predictions as an offset in the INLA-SPDE model, while the second (INLA-RF2) uses RF to directly correct selected latent field nodes. Both hybrid strategies enable uncertainty propagation between modeling stages, an aspect often overlooked in existing hybrid approaches. In addition, we propose a Kullback-Leibler divergence-based stopping criterion. We evaluate the predictive performance and uncertainty quantification capabilities of the proposed algorithms through two simulation studies. Results suggest that our hybrid approach enhances spatio-temporal prediction while maintaining interpretability and coherence in uncertainty estimates.

Keywords: Hybrid models, Integrated Nested Laplace Approximations, Random Forest, SPDE, Latent Gaussian Models, Uncertainty propagation

*Corresponding author

Email address: michela.cameletti@unibg.it (Michela Cameletti)

1. Introduction

Environmental phenomena are complex. They are usually observed at multiple time points and across various spatial locations, interacting with natural, physical and anthropogenic factors. When analyzing environmental data, the main goal is to understand hidden spatio-temporal patterns and to assess the relationship between predictors and the response variable. Additionally, predictive models enable prediction at new spatial locations or future time points.

Statistical models, such as Gaussian Process (GP) regression (Cressie and Wikle, 2011; Krainski et al., 2018; Wikle et al., 2019), are well-established tools widely applied in several environmental contexts, including air pollution prediction, ecological modeling and climate forecasting. These models rely on the likelihood function for inference ensuring a proper quantification of uncertainty. In particular, within a Bayesian framework, the well-established INLA-SPDE approach (Rue et al., 2009; Lindgren et al., 2011) provides a powerful parametric framework based on Latent Gaussian Models (LGM), enabling efficient and scalable inference while capturing spatio-temporal dependencies.

While statistical models are inherently interpretable, they may lack the flexibility needed to capture the complex, non-linear patterns and discontinuities that usually characterize environmental phenomena (Pichler and Hartig, 2023; Wikle and Zammit-Mangion, 2023; Agbehadji and Obagbuwa, 2024). In contrast, Machine Learning (ML) and Deep Learning (DL) models are particularly well-suited for modeling non-linear patterns and managing high-dimensional data. A key advantage of these methods is that they do not require to specify a functional form for the features-output relationship, as they learn directly from the data. However, they typically offer limited interpretability and lack native mechanisms for uncertainty quantification. More importantly, they are not able to exploit explicitly spatio-temporal correlation.

Hybrid models, which integrate statistical models with ML/DL methods, have recently emerged as a powerful approach (Wikle and Zammit-Mangion, 2023). These models combine the strengths of both paradigms: statistical methods offer interpretability and uncertainty quantification, while the flexibility of ML/DL methods can help in capturing complex non-linear relationships and high-dimensional dependencies. This synergy makes hybrid models particularly well-suited for modeling complex environmental data en-

hancing both the predictive capacity and the ability to uncover complex spatio-temporal patterns.

One common hybrid strategy, often referred to as residual learning, consists in applying sequentially two models: a first model is initially employed to fit the response variable, and subsequently, a second model is estimated on the first-stage residuals to capture any residual patterns that have not yet been captured. Typically, one of the two models belongs to the ML/DL group, while the other is a statistical model. The selection of the models and the order in which they are applied depend on the modeling objectives (e.g., [Fox et al., 2020](#); [de Mattos Neto et al., 2022](#); [Johnson et al., 2024](#); [Kakouri et al., 2025](#)). Another hybrid strategy is based on an ensemble approach, where statistical and ML/DL models make separate predictions that are then combined to produce the final output (e.g., see [Di et al., 2019](#); [Gheyas and Smith, 2011](#)). A third hybrid strategy is a hierarchical integration, with statistical and ML/DL models embedded within a single hierarchical framework. For instance, the BAYESNF algorithm proposed by [Saad et al. \(2024\)](#) integrates a Neural Network (NN) architecture with hierarchical Bayesian inference, giving rise to a Bayesian NN model with prior distributions assigned to the parameters of the network.

The aim of this paper is to enhance the predictive accuracy of statistical spatio-temporal models, estimated via the INLA-SPDE approach, by proposing a hybrid modeling strategy that preserves interpretability and uncertainty quantification. We thus introduce two novel algorithms, collectively named INLA-RF, which combine a parametric GP-based spatio-temporal model with a well-established ML algorithm as Random Forest (RF). The two models adopt a two-stage iterative scheme, with the statistical model capturing the spatio-temporal structure and the RF enhancing predictive flexibility. Our proposal aligns with the residual learning hybrid strategy but extends it by incorporating uncertainty propagation between the two modelling stages, addressing a critical aspect that is commonly overlooked in existing approaches.

In the first algorithm —INLA-RF with offset correction (hereafter referred to as INLA-RF1)— RF predictions are incorporated into the statistical model as a known offset, effectively providing information about the mean structure of the response variable, while the INLA-SPDE model accounts for the spatio-temporal correlation. This strategy is inspired by [MacBride et al. \(2025\)](#), who introduced the SPAR-Forest algorithm combining RF with well-known spatial models for areal data, as the Conditional Autoregressive

(CAR) or Spatial Autoregressive (SAR) models. Differently from [MacBride et al. \(2025\)](#), we focus on point-referenced data, consider a different order for the two combined models and also propose a strategy for propagating the uncertainty of the RF predictions into the parametric model.

The second algorithm —INLA-RF with latent field nodes correction (hereafter referred to as INLA-RF2)— goes a step further and makes use of the RF predictions to correct the latent field nodes in the INLA-SPDE model by means of an extra random effect. In this way, the RF information contributes to the latent field while still embedding the spatio-temporal correlation and enabling full uncertainty propagation. The nodes to be corrected are chosen according to criteria that identify where the current model is most uncertain or least accurate ensuring that the hybrid model focuses where it is most needed.

For both algorithms we use the Kullback-Leibler divergence (KLD) as a stopping criterion, proposing three different ways for calculating it in the INLA-SPDE framework. As a result, the number of iterations is not a tuning parameter, as it is in [MacBride et al. \(2025\)](#), but is instead determined by an empirical measure of how much the posterior distribution changes between iterations. This approach can improve computational efficiency, by avoiding unnecessary iterations, and reduce the risk of overfitting.

We evaluate the predictive performance of our algorithms through two simulation studies, using as a benchmark a base INLA-SPDE model without hybridization. The results suggest that the INLA-RF algorithms provide improved predictive performance, especially in the presence of temporal discontinuities or non-linear relationships between covariates and the response.

The paper is structured as follows. In [Section 2.1](#) we introduce the spatio-temporal framework we work in. The INLA-SPDE approach and the RF algorithm are described in [Section 2.2](#) and [2.3](#), respectively. The core of the paper is presented in [Section 2.4](#), where our two novel INLA-RF algorithms are detailed and illustrated using pseudo-code. Two simulation studies are discussed in [Section 3](#), while [Section 4](#) concludes the paper with a discussion and final remarks. In [Appendix A](#) we provide the results of the structured k -fold Cross-Validation (CV) analysis - using spatio-temporal CV blocks - conducted for the first simulation study.

2. Methodology

2.1. Parametric spatio-temporal modeling

We denote by $y(\mathbf{s}_i, t)$ the response variable at the i -th location (with coordinates $\mathbf{s}_i \in \mathbb{R}^2$, $i = 1, \dots, n$) and time $t \in \mathbb{N}$ ($t = 1, \dots, T$). Considering all the locations and time points we obtain the following response vector

$$\mathbf{y} = (y(\mathbf{s}_1, 1), \dots, y(\mathbf{s}_n, 1), \dots, y(\mathbf{s}_1, T), \dots, y(\mathbf{s}_n, T))^T,$$

where T is the transpose operator. Moreover, $\mathbf{z}(\mathbf{s}_i, t) = (z_1(\mathbf{s}_i, t), \dots, z_P(\mathbf{s}_i, t))^T$ represents the location-time specific P -dimensional covariate vector.

We assume that the data are a function of the so-called large-scale component (LS), depending on the covariates, and a random effects (REs) term that includes spatial and temporal dependence, plus the measurement noise:

$$y(\mathbf{s}_i, t) = LS(\mathbf{s}_i, t) + RE(\mathbf{s}_i, t). \quad (1)$$

A common approach in statistical modeling is to assume that the LS component in Eq. (1) is a linear function of the P covariates (i.e., $LS(\mathbf{s}_i, t) = \boldsymbol{\beta} \mathbf{z}(\mathbf{s}_i, t)$, where $\boldsymbol{\beta}$ is the vector of fixed effect coefficients) and that the REs term is given by the sum of a Gaussian unstructured (IID) measurement error $\epsilon(\mathbf{s}_i, t)$ and of a spatio-temporal Gaussian process $\omega(\mathbf{s}_i, t)$. The latter can be specified hierarchically in different ways (Wikle et al., 2019); however, at each time point, it generally results in a zero-mean multivariate Gaussian distribution with a dense covariance matrix, whose entries are determined by the spatio-temporal covariance function. For this reason, the estimation of such a model can be computationally challenging, especially when dealing with a large number of spatial locations. A viable solution for this computational challenge, also known as *big n problem* (Jona Lasinio et al., 2013), is represented by the INLA-SPDE approach described in Section 2.2. It has been proved (Lindgren et al., 2011, 2022) as a valid and computationally efficient solution for fast model estimation and spatial prediction. In particular, since the INLA-SPDE approach adopts a Bayesian framework, it provides posterior distributions for all unknown parameters, including the structured random effects. Moreover, it allows for posterior predictive distributions of the response variable, enabling spatial prediction at any location within the domain.

2.2. The INLA-SPDE approach

INLA is a deterministic approximate Bayesian inference approach grounded in the properties of the Gaussian Markov Random Field (GMRF) and its computational efficiency. This methodology was developed by Rue et al. (2009), implemented in R through the R-INLA package (<https://www.r-inla.org/>), and later extended to more flexible modeling structures (Lindgren and Rue, 2015; Bakka et al., 2018; Krainski et al., 2018; Gómez-Rubio, 2020; Van Niekerk and Rue, 2024). This approach allows Bayesian inference to be performed on a wide range of structured additive models, known as LGMs. While INLA primarily focuses on computing marginal posterior distributions, it effectively addresses the challenges of determining the joint posterior distributions of interest through a series of nested approximations or a low-rank variational Bayes correction for the latent field (Van Niekerk et al., 2023; Van Niekerk and Rue, 2024). This technique enables the computation of marginal likelihoods, standard goodness-of-fit metrics (DIC, WAIC, CPO), cross-validation checks, and posterior predictive distributions.

Since INLA is based on GMRF principles, it offers inherent computational efficiency when modeling data with conditional independence. Generally speaking, given the vector of n observations $\mathbf{y} = (y_1, \dots, y_n)$, the likelihood, assuming conditional independence, is described by the following expression:

$$\pi(\mathbf{y}|\boldsymbol{\eta}, \boldsymbol{\theta}) = \prod_{i=1}^n \pi(y_i | \eta_i, \boldsymbol{\theta}), \quad (2)$$

where η_i is the i^{th} component of the linear predictor vector $\boldsymbol{\eta} = (\eta_1, \dots, \eta_n)$, which includes fixed and random effects, and is defined¹ as follows (Lindgren and Rue, 2015):

$$\eta_i = \sum_k h_k(z_i^k), \quad (3)$$

where $h_k(\cdot)$ is known as mapping function. In the case of a fixed effect z_i^k is given by the covariate value included in the linear predictor through a linear function, i.e., $h_k(z_i^k) = \beta_k z_i^k$. In the case of a random effect z_i^k defines the unit index (e.g., the grouping, spatial or temporal index) and $h_k(z_i^k) = u_k(z_i^k)$, where u_k is the value of the latent Gaussian variable assumed for the random

¹Given that we assume the Gaussian distribution for the response variable it results that $E(y_i) = \eta_i$, i.e., we are using an identity link function.

effect (with a structured or unstructured prior distribution). The latent field \mathbf{x} encompasses all the latent Gaussian variables which are part of the linear predictor, including the vector of fixed effect coefficients $\boldsymbol{\beta}$ used to include linear effects of the covariates. It is assumed that the latent field \mathbf{x} follows a multivariate normal prior distribution with mean $\boldsymbol{\mu}$, usually equal to $\mathbf{0}$, and precision matrix $\mathbf{Q}(\boldsymbol{\theta}_2)$. Given the conditional independence property, it follows that this precision matrix is sparse and this allows for computationally efficiency when performing matrix operations (Rue and Held, 2005). The vector of hyperparameters is given by $\boldsymbol{\theta} = (\boldsymbol{\theta}_1, \boldsymbol{\theta}_2)$, where $\boldsymbol{\theta}_1$ refers to the likelihood hyperparameters and $\boldsymbol{\theta}_2$ to the latent field hyperparameters.

The INLA methodology exploits the assumptions of the model to produce a numerical approximation to the posterior distribution of interest, i.e., the joint posterior distribution of the hyperparameters $\pi(\boldsymbol{\theta} \mid \mathbf{y})$ and the latent field marginal distribution $\pi(x_i \mid \mathbf{y})$.

In Eq. (3) each term $h_k(z_i^k)$ represents the contribution to the linear predictor of a component (also named node) of the latent field \mathbf{x} . As explained in Lindgren and Rue (2015), this formulation only allows each observation to be linked to one element from each $h_k(\cdot)$ effect. This can be a limitation when each observation depends on multiple components of \mathbf{x} , as it is the case of spatial random effects. To deal with this, the projection matrix \mathbf{A} is introduced as the design matrix of the model, incorporating covariate values, factor structures and their levels, and weights associated with random effects (e.g., basis weights for spatial effects); it basically defines how each observation is linked to the latent field components. Eq. (3) can thus be rewritten as

$$\eta_i = \sum_{j=1}^J \mathbf{A}_{ij} x_j,$$

where \mathbf{A}_{ij} is the weight of the j^{th} component of the latent field contributing to the linear predictor η_i for the i^{th} observation. Note that the total number of latent components J depends on the model structure. In matrix notation we have that $\boldsymbol{\eta} = \mathbf{A} \mathbf{x}$. In the following sections we will use the notation $\text{LGM}(\mathbf{A}, \mathbf{x}, \boldsymbol{\theta})$ to identify an unique LGM model structure.

The R-INLA package implements also the Stochastic Partial Differential Equation (SPDE) technique, introduced by Lindgren et al. (2011) for modeling point-referenced spatial data in a computationally efficient way (see also Lindgren and Rue 2015; Krainski et al. 2018; Lindgren et al. 2022). This method exploits the fact that the solution to a specific SPDE is a Gaussian

Field (GF) with Matérn covariance function (see Eq. (10)). The novelty of the SPDE approach is to represent the Matérn GF as a GMRF by using the finite element method, i.e. by defining the Matérn field as a linear combination of basis functions defined on a triangulation (i.e., mesh) of the considered spatial domain (see for example Figure 1). This eliminates the need to work with a dense covariance matrix and instead allows the use of a sparse precision matrix, avoiding computationally expensive inversion processes. Note that when applying the SPDE approach in a two-dimensional spatial domain, the Matérn smoothness parameter ν is set equal to one and the spatial range is given by $\rho = \sqrt{8\nu}/\kappa$ and interpreted as the distance at which the correlation drops to approximately 0.13 (see Lindgren et al., 2011).

The linear combination of basis functions used to approximate a Matérn GF $\xi(\mathbf{s})$ is given by

$$\xi(\mathbf{s}) = \sum_{g=1}^G \psi_g(\mathbf{s}) \tilde{\xi}_g, \quad (4)$$

where G is the total number of mesh vertices, $\psi_g(\cdot)$ are piecewise linear basis functions, and $\tilde{\boldsymbol{\xi}} = (\tilde{\xi}_1, \dots, \tilde{\xi}_G)$ are latent weights modeled as a multivariate zero-mean Gaussian random variable with a sparse precision matrix derived from the SPDE formulation (that's why $\tilde{\boldsymbol{\xi}}$ is a GMRF). When implementing the SPDE approach with INLA, the summation in Eq. (4) is used as one of the components of the linear predictor defined in Eq. (3), as an indexed random effect. Accordingly, the latent Gaussian vector $\tilde{\boldsymbol{\xi}}$ will be included in the INLA latent field \mathbf{x} (Lindgren and Rue, 2015). In this case the projector matrix \mathbf{A} (with dimension $n \times G$) maps the GMRF $\tilde{\boldsymbol{\xi}}$ from the G mesh vertices to the n observation locations such that $\mathbf{A}_{ig} = \psi_g(\mathbf{s}_i)$. In particular, when a spatial location \mathbf{s}_i lies within a triangle defined by three mesh vertices, the corresponding row of \mathbf{A} contains three nonzero elements, which sum to one (Krainski et al., 2018).

2.3. Random Forest

Random Forest (RF, Breiman, 2001) is a widely adopted non-parametric ML model which has gained notoriety given its simple implementation and the satisfactory predictive results. The RF algorithm is based on two main elements: bootstrap (Efron, 1979) and decision trees (Breiman et al., 1984). The two methods interact in the following way: B bootstrapped samples are generated from the available data, and a decision tree is fitted on each of them. Decision tree growth is an iterative process in which the predictor

space is partitioned at each step until a stopping rule is satisfied. The splitting optimization algorithm determines the best predictor and corresponding cut off value to minimize local residual errors. In the specific case of RF, the optimal predictor is selected from a randomly chosen subset of the original variables (see, e.g., [James et al., 2021](#)). Being based on decision trees, RF is characterized by high flexibility in modeling the relationship between predictors and the response variable, being able to capture non-linear relationships and interactions between and within predictors.

The issue with employing RF in applications involving correlated data is its inability to account for spatial and/or temporal correlation between observations. It means that RF can be effectively used only to estimate the LS component of Eq. (1). This limitation arises from the fact that the RF bootstrap does not consider, when creating samples, information coming from the spatial location or temporal indexing of the observations. Additionally, in the absence of spatial and/or temporal information introduced through predictors, the splitting mechanism cannot leverage them. In [Patelli et al. \(2024\)](#), a comprehensive literature review was conducted to identify the adopted strategies to make RF spatially aware, and these strategies were then systematically organized following a taxonomy. A synthesis of these strategies reveals three main categories, distinguished by when spatial information is incorporated into the RF predictive process (at the covariates level, modifying the internal algorithm or as a post-processing phase). Among the identified contributions, RF-GLS ([Saha et al., 2023](#)) appears to be the most promising because it incorporates spatial correlation during the tree growth. However, it appears to be computationally intensive ([Heaton et al., 2024](#)) and constrained to the case of purely spatial or temporal dependency structure. Consequently, it is not suitable for spatio-temporal applications. Another limitation of RF is that, being a non-parametric method, it lacks direct interpretability and uncertainty evaluation of the predictions.

2.4. *INLA-RF algorithms*

In this section we describe the two hybrid modeling strategies we propose, named INLA-RF algorithms, which iteratively combine a base spatio-temporal model as described in Section 2.1, estimated using the INLA-SPDE approach (here after simply referred to as INLA model), with the RF algorithm presented in Section 2.3. The key idea is to alternate between the spatio-temporal model (STEP 1) and the RF algorithm (STEP 2), which is applied to the residuals of the first model. In turn, the statistical model

incorporates information coming from the RF output. We expect that this integration leverages the RF ability to capture complex non-linear patterns and discontinuities in the residuals that the parametric model may miss, thereby enhancing the predictive capability. This information is then incorporated back in the statistical INLA model which is the benchmark approach in terms of interpretability and ability to estimate uncertainty, two issues that RF is not able to address.

The two proposed modeling strategies are described in the following sections and detailed in Algorithm 1 and 2 using pseudo-code. For simplicity here onward we omit the spatial and temporal indexes and denote $y(\mathbf{s}_i, t)$ as y ; the bold notation is used for vectors and matrices.

2.4.1. INLA-RF1: offset correction (without and with uncertainty propagation)

This approach is quite intuitive and takes inspiration by what was proposed in MacBride et al. (2025) for the case of areal data. In particular, the RF output is incorporated into the INLA model as an offset term whose uncertainty can be taken into account or not. In detail, the generic i^{th} iteration implements the following two steps (see Algorithm 1):

1. **STEP 1:** we run the base INLA model including the RF output from the previous step (given by $\hat{\mathbf{e}}_{RF}^{(i-1)}$) as offset. The latter is a known constant that shifts the linear predictor and operates like a correction of the mean. This is equivalent to fit the LGM model on the residuals $\mathbf{y} - \hat{\mathbf{e}}_{RF}^{(i-1)}$ between the observed values of the response variable and the RF predictions. We obtain as output of the INLA estimation the posterior mean and precision matrix of the latent field \mathbf{x} , denoted by $\boldsymbol{\mu}^{(i)}$ and $\mathbf{Q}^{(i)}$, respectively. The latter are needed to evaluate the stopping condition based on the Kullback-Leibler divergence. Finally, the INLA residuals given by $\hat{\mathbf{e}}_{INLA}^{(i)} = \mathbf{y} - \hat{\mathbf{y}}_{INLA}^{(i)}$ are computed, where the predictions $\hat{\mathbf{y}}_{INLA}^{(i)}$ are given by the posterior mean of the predictive distributions.
2. **STEP 2:** we run the RF algorithm using as response variable the INLA residuals $\hat{\mathbf{e}}_{INLA}^{(i)}$ and as predictors the actual regressors used in STEP 1 together with the time index and the spatial coordinates. As an output we get the RF predictions for the residuals denoted by $\hat{\mathbf{e}}_{RF}^{(i)}$.

The two steps are repeated until the stopping condition $D_{KL} < \delta$ is met, where D_{KL} is based on the Kullback-Leibler divergence (KLD, Kullback,

1997), and δ is a tolerance threshold (see Section 2.4.3 for the details about the computation of D_{KL}). If D_{KL} is lower than δ , it suggests that there is no significant difference in the posterior distribution of the latent field between two consecutive iterations, and further correction is not needed. At the first iteration ($i = 0$) the algorithm is initialized as follows: $\hat{\mathbf{e}}_{RF} = \mathbf{0}$, $D_{KL} = 10$, $\delta = 0.01$. Moreover, the initial values for $\boldsymbol{\mu}^{(0)}$, $\mathbf{Q}^{(0)}$ are obtained from an initial fit of the INLA model fitted with the response variable data \mathbf{y} and including all the available predictors.

An important issue when combining the two models is related to uncertainty propagation. By default the offset (used in STEP 1) is assumed to be a fixed quantity, given by the RF output, which should adjust the INLA estimation. However, this does not take into account the RF prediction uncertainty. Actually, the offset itself has its own variability coming from the RF algorithm and given by the overall out-of-bag (OOB) prediction error (computed as the OOB mean squared error and denoted by $\hat{\sigma}_{RF}^2$). In order to propagate the RF uncertainty into the SPDE model, we can exploit the fact that the INLA algorithm allows to treat the offset as a random quantity with a known precision, in this case given by $1/\hat{\sigma}_{RF}^2$. This means that if the RF predictions are highly uncertain, the INLA model will down-weight the offset correction. From a practical point of view, INLA updates the likelihood precision τ including the offset uncertainty so that $\tau \leftarrow (1/\tau + \hat{\sigma}_{RF}^2)^{-1}$.

The final output of Algorithm 1 is the last implemented STEP 1 integrating the RF correction ($\hat{\mathbf{e}}_{RF}$, $\hat{\sigma}_{RF}^2$) from the last STEP 2.

Algorithm 1 INLA-RF hybrid approach: offset approach (without and with uncertainty propagation)

State 1: Run a first LGM($\mathbf{A}, \mathbf{x}, \boldsymbol{\theta}$) using \mathbf{y} and obtain $\boldsymbol{\mu}^{(0)}$ and $\mathbf{Q}^{(0)}$.

State 2: Initialize the INLA-RF algorithm with $i = 0$, $D_{KL} = 10$, $\delta = 0.01$, $\hat{\mathbf{e}}_{RF}^{(0)} = \mathbf{0}$, $\hat{\sigma}_{RF}^{2(0)}$.

while $D_{KL} \geq \delta$ **do**

if $i \geq 1$ **then**

STEP 1: integrate the RF output $\hat{\mathbf{e}}_{RF}^{(i-1)}$ as offset; i.e., run the LGM($\mathbf{A}, \mathbf{x}, \boldsymbol{\theta}$) with $\mathbf{y} \leftarrow \mathbf{y} - \hat{\mathbf{e}}_{RF}^{(i-1)}$.

if *uncertainty propagation* == *TRUE* **then**

 Add the estimate of uncertainty from RF ($\hat{\sigma}_{RF}^{2(i-1)}$) as an offset to the precision τ of the likelihood: $\tau \leftarrow (1/\tau + \hat{\sigma}_{RF}^{2(i-1)})^{-1}$.

end

 Obtain $\boldsymbol{\mu}^{(i)}$ and $\mathbf{Q}^{(i)}$.

 Compute D_{KL} .

end

 Compute the INLA residuals $\hat{\mathbf{e}}_{INLA}^{(i)} = \mathbf{y} - \hat{\mathbf{y}}_{INLA}^{(i)}$.

STEP 2: Implement RF with $\hat{\mathbf{e}}_{INLA}^{(i)}$ as response and predict $\hat{\mathbf{e}}_{RF}^{(i)}$.

$i = i + 1$

end

Output: Output from the last implemented STEP 1 integrating the RF correction ($\hat{\mathbf{e}}_{RF}$, $\hat{\sigma}_{RF}^2$) from the last STEP 2.

2.4.2. INLA-RF2: latent field nodes correction

The second INLA-RF hybrid approach we propose uses the RF output to correct specific nodes (here after also denoted as stress points) of the latent field \mathbf{x} by defining new nodes—one for each node to be corrected—within the LGM. This is a completely new approach which uses the RF output to perform a localized correction of the random effects, instead of working on a mean correction of the linear predictor as Algorithm 1 does. Moreover, differently from Algorithm 1, it propagates automatically uncertainty across the two steps.

Also in this case we alternate two steps, with STEP 1 making use of the base INLA model and STEP 2 being based on a RF run. Before starting with the iterative while loop, a first base INLA model (LGM($\mathbf{A}, \mathbf{x}, \boldsymbol{\theta}$) with \mathbf{y}) is run, and based on its results the latent field nodes to be corrected are

identified. We thus define the set $\mathbf{x}_c = \{x_k, k \in \mathcal{K}\}$, where \mathcal{K} is the set of indices identifying the nodes of the latent field \mathbf{x} to be corrected. Note that the cardinality of \mathcal{K} , denoted by $|\mathcal{K}|$ is defined in advance (e.g., $|\mathcal{K}| = 100$). The selection of nodes can be made according to different criteria recalling that the latent field \mathbf{x} is linked to the linear predictor through $\boldsymbol{\eta} = \mathbf{A} \mathbf{x}$ (see Section 2.2) and that it is assumed to be a GMRF. For example, we could consider the variance of the marginal distribution of each latent field node (i.e., $\text{Var}(x_i | \mathbf{y})$) or the RMSE associated with the mean of the posterior predictive distribution (given by the linear predictor η_i). In the first case, nodes with the highest variances in the latent field should be chosen, while in the second case nodes in the linear predictor with the highest RMSE values should be identified. Recall that the latent field \mathbf{x} contains all the fixed and random effects defining the model (see Section 2.2); it is then necessary to define which nodes have to be corrected, e.g., those related to spatial or temporal structures or the random effects associated with a covariate.

The correction applied to each node must be performed at its corresponding “location” —i.e., the associated index— since in the INLA model, random effect nodes are defined through a GMRF, which can be interpreted as a graph over a discrete index set. In a spatial modeling context, the projector matrix \mathbf{A} enters into play to define a mapping between the GMRF nodes and the observation locations where the RF predictions are available. The same logic applies in a temporal context, where the GMRF indices might correspond to years, months, or other temporal points; even when the temporal data is already discretized, corrections must still be applied using the RF predictions at the locations associated with the temporal nodes to be adjusted.

As mentioned before, for each node to be corrected a new additional node will be defined (in the same “locations” \mathcal{K}). This will give rise to a new random effect, given by the vector of extended nodes, denoted by \mathbf{x}'_c . In particular, an IID prior distribution (i.e., a diagonal precision matrix scaled by a precision parameter) will be assumed for \mathbf{x}'_c :

$$\mathbf{x}'_c \sim \text{MVN}(\boldsymbol{\mu}'_c, \tau'_c \mathbf{I}),$$

where the mean vector and the precision are updated using the RF output.

In particular, at the i^{th} iteration of the algorithm we have that

$$\begin{aligned} \boldsymbol{\mu}'_c^{(i)} &= \boldsymbol{\mu}'_c^{(i-1)} + \hat{\mathbf{e}}_{RF}^{(i-1)} \\ \tau'_c{}^{(i)} &= \left(\sigma_{RF}^2{}^{(i-1)} \right)^{-1} \end{aligned} \tag{5}$$

with $\hat{\mathbf{e}}_{RF}^{(i-1)}$ being the predictions from the RF algorithm obtained at the previous iteration at the “locations” of the nodes to be corrected, and $\sigma_{RF}^{2(i-1)}$ the corresponding OOB RF prediction error. From a practical point of view, in INLA all the random effects are assumed to have a mean equal to zero. This means that $\boldsymbol{\mu}'_c$ will be provided through an offset vector, which will be equal to zero for all the elements of the linear predictor except for the nodes that are being corrected.

To recap the generic i^{th} iteration of Algorithm 2:

1. in **STEP 1** we use the RF output $\hat{\mathbf{e}}_{RF}^{(i-1)}$ to define the parameters of the distribution of $\mathbf{x}'_c^{(i)}$ (see Eq. (5)). Using \mathbf{y} we will then estimate the enlarged LGM given by $(\{\mathbf{A}, \mathbf{A}_c\}, \{\mathbf{x}, \mathbf{x}'_c^{(i)}\}, \boldsymbol{\theta})$ which includes the new IID random effect \mathbf{x}'_c taking care of correcting the nodes. The projection matrix \mathbf{A}_c identifies which are the nodes to be corrected. As in Algorithm 1, we conclude the first step by computing the INLA predictions and residuals $\hat{\mathbf{e}}_{INLA}^{(i)} = \mathbf{y} - \hat{\mathbf{y}}_{INLA}^{(i)}$, and by obtaining $\boldsymbol{\mu}^{(i)}$ and $\mathbf{Q}^{(i)}$ which are needed for computing D_{KL} and evaluating the stopping criterion (see Section 2.4.3).
2. In **STEP 2** the RF algorithm is run using the INLA residuals $\hat{\mathbf{e}}_{INLA}^{(i)}$ as response variable and the time index together with the spatial coordinates as predictors. As output we get the predictions for the residuals denoted by $\hat{\mathbf{e}}_{RF}^{(i)}$.

The final output of Algorithm 2 results from the last implemented STEP 1 with the INLA-based estimation and the RF correction to the specified nodes already integrated.

Algorithm 2 INLA-RF hybrid approach: latent field nodes correction

State 1: Run a first base LGM($\mathbf{A}, \mathbf{x}, \boldsymbol{\theta}$) using \mathbf{y} and obtain $\boldsymbol{\mu}^{(0)}$ and $\mathbf{Q}^{(0)}$.

State 2: Set $|\mathcal{K}|$ and determine the nodes to be corrected $\mathbf{x}_c = \{x_k, k \in \mathcal{K}\}$.

State 3: Initialize the INLA-RF algorithm with $i = 0$, $D_{KL} = 10$, $\delta = 0.01$, $\hat{\mathbf{e}}_{RF}^{(0)} = \mathbf{0}$, $\boldsymbol{\mu}'_c = \mathbf{0}$ and $\tau'_c = 0$.

while $D_{KL} \geq \delta$ **do**

if $i \geq 1$ **then**

STEP 1: use the RF output to update the distribution of the extended nodes: $\mathbf{x}'_c{}^{(i)} \sim \text{MVN}\left(\boldsymbol{\mu}'_c{}^{(i)}, \tau'_c{}^{(i)} \mathbf{I}\right)$, where $\boldsymbol{\mu}'_c{}^{(i)} = \boldsymbol{\mu}'_c{}^{(i-1)} +$

$\hat{\mathbf{e}}_{RF}^{(i-1)}$ and $\tau'_c{}^{(i)} = \left(\sigma_{RF}^2{}^{(i-1)}\right)^{-1}$

 Run the extended LGM ($\{\mathbf{A}, \mathbf{A}_c\}, \{\mathbf{x}, \mathbf{x}'_c{}^{(i)}\}, \boldsymbol{\theta}$) using \mathbf{y} .

 Obtain $\boldsymbol{\mu}^{(i)}$ and $\mathbf{Q}^{(i)}$.

 Compute D_{KL} .

end

 Compute the INLA residuals $\hat{\mathbf{e}}_{INLA}^{(i)} = \mathbf{y} - \hat{\mathbf{y}}_{INLA}^{(i)}$.

STEP 2: Implement RF with $\hat{\mathbf{e}}_{INLA}^{(i)}$ as response and predict $\hat{\mathbf{e}}_{RF}^{(i)}$.

$i = i + 1$

end

Output: Output from the last implemented STEP 1.

2.4.3. Stopping criterion

The value of D_{KL} can be computed using two different approaches: (1) using the KLD given by the conditional posterior distribution of the latent field in the modal configuration of the hyperparameters, or (2) using the KLD given by the marginal posterior distribution of the latent field. In the following, the notation $KLD(\cdot||\cdot)$ is used to denote the KLD between two distributions.

The first approach accounts for the “average” Kullback-Leibler divergence between two multivariate distributions, i.e., the KLD accounts for the dimension of the latent field. In the INLA methodology the joint conditional posterior distribution $\pi(\mathbf{x} | \mathbf{y}, \boldsymbol{\theta})$ is computed as a Gausssian approximation,

which allows us to compute the D_{KL} at a low computational cost as follows:

$$\begin{aligned}
D_{KL} &= KLD \left(\pi(\mathbf{x} \mid \mathbf{y}^{(i-1)}, \boldsymbol{\theta}^{(i-1)}) \parallel \pi(\mathbf{x} \mid \mathbf{y}^{(i)}, \boldsymbol{\theta}^{(i)}) \right) \\
&= \frac{1}{2} \left((\boldsymbol{\mu}^{(i)} - \boldsymbol{\mu}^{(i-1)})^T \mathbf{Q}^{(i)} (\boldsymbol{\mu}^{(i)} - \boldsymbol{\mu}^{(i-1)}) + \text{tr}(\mathbf{Q}^{(i)} \mathbf{Q}^{(i-1)^{-1}}) - \log \frac{|\mathbf{Q}^{(i)}|}{|\mathbf{Q}^{(i-1)}|} \right), \tag{6}
\end{aligned}$$

where T is the transpose operation, tr is the matrix trace and $|\cdot|$ the determinant. Moreover, $\pi(\mathbf{x} \mid \mathbf{y}^{(i)}, \boldsymbol{\theta}^{(i)})$ is the conditional posterior distribution at the i^{th} iteration. Therefore, $\pi(\mathbf{x} \mid \mathbf{y}^{(i)}, \boldsymbol{\theta}^{(i)})$ follows a multivariate Gaussian distribution denoted by $\text{MVN}(\boldsymbol{\mu}^{(i)}, \mathbf{Q}^{(i)})$, with mean vector $\boldsymbol{\mu}^{(i)}$ and precision matrix $\mathbf{Q}^{(i)}$.

The second approach is computed as average difference in the marginal posterior distributions of all the latent field components (or nodes) represented by $\pi(x_j \mid \mathbf{y}^{(i-1)})$:

$$D_{KL} = \frac{1}{J} \sum_{j=1}^J KLD \left(\pi(x_j \mid \mathbf{y}^{(i-1)}) \parallel \pi(x_j \mid \mathbf{y}^{(i)}) \right), \tag{7}$$

with J being the total number of latent field components.

Alternatively, instead of using an average measure we can consider the maximum KLD computed over the set of latent field nodes denoted by \mathcal{J} . This measure is defined as follows:

$$D_{KL} = \max_{j \in \mathcal{J}} \left\{ KLD \left(\pi(x_j \mid \mathbf{y}^{(i-1)}) \parallel \pi(x_j \mid \mathbf{y}^{(i)}) \right) \right\}. \tag{8}$$

This has the advantage of controlling whether every node update remains below the threshold δ . Note that it can also be computed considering a subset of nodes ($\mathcal{J}' : \mathcal{J}' \subset \mathcal{J}$) if we are interested in evaluating the changes in the marginal distributions only for the nodes in the subset \mathcal{J}' .

3. Simulation studies

To evaluate the performance of our hybrid modeling approaches (described in Algorithm 1 and 2), we conduct two simulation studies. The first is a spatio-temporal example which compares the INLA-RF1 algorithm against a spatio-temporal model with no hybridization. The second is a

purely temporal scenario designed to assess the INLA-RF2 approach in modeling temporal discontinuities.

The code to replicate the results is available at the <https://github.com/LucaPate/INLA-RF/tree/main> GitHub repository.

3.1. Spatio-temporal simulation study for INLA-RF1

In the first simulation study, we simulate a dataset with $T = 8$ time points and $n = 150$ spatial locations per each time location, assuming that the spatial locations are changing in time in the given spatial domain (see Figure 1). The study region and the spatial locations refer to the Paraná state and are available in the R INLA package (Krainski et al., 2018). We simulate the data using the following spatio-temporal model which is widely adopted in the environmental modeling literature (see e.g., Cameletti et al., 2013; Moraga, 2019; Wikle et al., 2019; Fioravanti et al., 2021, 2022, 2023; Otto et al., 2024). We consider two quantitative predictors (z_1 and z_2) and one categorical regressor with three classes included using dummy variables (D_1 , D_2 and D_3 with coefficients γ_1 , γ_2 and γ_3 , respectively) which enters in the model through two non-linear functions $f_1(\cdot)$ and $f_2(\cdot)$:

$$y(\mathbf{s}_i, t) = f_1(z_1(\mathbf{s}_i, t)) + f_2(z_2(\mathbf{s}_i, t)) + \sum_{j=1}^3 \gamma_j D_j(\mathbf{s}_i, t) + \omega(\mathbf{s}_i, t) + \epsilon(\mathbf{s}_i, t)$$

$$\omega(\mathbf{s}_i, t) = a\omega(\mathbf{s}_i, t-1) + \xi(\mathbf{s}_i, t).$$
(9)

The measurement error is assumed to be normally distributed, i.e., $\epsilon(\mathbf{s}_i, t) \sim N(0, \sigma_\epsilon^2)$, while the latent process $\omega(\mathbf{s}_i, t)$ is characterized by a first order autoregressive temporal dynamics (AR(1)) with coefficient a and by spatially correlated innovations. In particular, $\xi(\mathbf{s}_i, t)$ is assumed to be a zero-mean Gaussian (isotropic and second order stationary) process with spatio-temporal covariance function given by

$$\text{Cov}(\xi(\mathbf{s}_i, t_k), \xi(\mathbf{s}_j, t_l)) = \begin{cases} 0, & \text{for } t_k \neq t_l \\ \mathcal{C}(h), & \text{for } t_k = t_l \end{cases},$$

where $h = \|\mathbf{s}_i - \mathbf{s}_j\| \in \mathbb{R}$ is the Euclidean distance and $\mathcal{C}(h)$ is the Matérn spatial covariance function defined as follows (Wikle et al., 2019):

$$\mathcal{C}(h) = \sigma^2 \frac{2^{1-\nu}}{\Gamma(\nu)} (\kappa h)^\nu \mathcal{K}_\nu(\kappa h). \quad (10)$$

The term σ^2 is the spatial variance and \mathcal{K}_ν is the modified Bessel function of the second kind of order $\nu > 0$, the latter being the parameter that controls the smoothness of the spatial process. The term $\kappa > 0$ is a scaling parameter related to the spatial range ρ , represented by the distance at which the spatial correlation is negligible.

For the simulation we set $\gamma_1 = 0.727$, $\gamma_2 = -1.027$ and $\gamma_3 = 0.3$. The values of z_1 are drawn from a standard Normal distribution with $f_1(\cdot)$ being a non-linear function given by $f_1(z_1) = 2z_1 \sin(2z_1)$. Finally, z_2 is simulated from a Uniform distribution defined between 0 and 1 with $f_2(\cdot)$ being another non-linear function defined as $f_2(z_2) = \sin(z_2^4) + \cos(2.5\pi z_2)$. Given that the response variable depends on the two quantitative predictors through non-linear functions, we expect our hybrid algorithms to perform better than a model that assumes a linear function of the covariates.

For the spatial covariance function we assume $\sigma^2 = 1$ and $\rho = 3.627$ (given by half the maximum distance for the considered domain). The measurement error ϵ is assumed to be a mean-zero Gaussian process with variance set equal to $\sigma_\epsilon^2 = 1/50 = 0.02$. Finally, for the AR(1) part we assume $a = 0.7$. The simulated data, for the considered 8 time points, are displayed in Figure 1 together with the SPDE mesh.

The prior distributions for Bayesian inference were chosen to be vague for the fixed effects, using Gaussian priors with high variance, i.e. $N(0, \sigma^2 = 1/0.001)$. For the spatio-temporal interaction effect, we have three hyperparameters: σ , ρ and a . For σ and ρ , we use Penalized Complexity (PC) priors (Simpson et al., 2017; Fuglstad et al., 2019), specified as $P(\sigma > \sigma_0) = 0.5$ and $P(\rho < \rho_0) = 0.5$, where $\sigma_0 = 1$ and ρ_0 is set to the maximum distance (d) between two points on the boundary of the study region divided by 5, i.e., $\rho_0 = d/5$. Finally, the prior distribution for the temporal autocorrelation parameter is defined as $\text{logit}(a) \sim N(0, 0.15)$.

In the implementation of Algorithm 1, both with and without uncertainty propagation, we made use of the first KLD stopping criterion (see Eq. (6)).

3.1.1. Results

In this section, we compare the INLA-RF1 approach - both with and without uncertainty propagation - to a base INLA model similar to Eq. (9), but assuming a linear relationship for the regressors. The base INLA model serves as a benchmark.

The used performance metrics are Root Mean Square Error (RMSE), Mean Absolute Error (MAE), Coverage Probability (CP), and Average In-

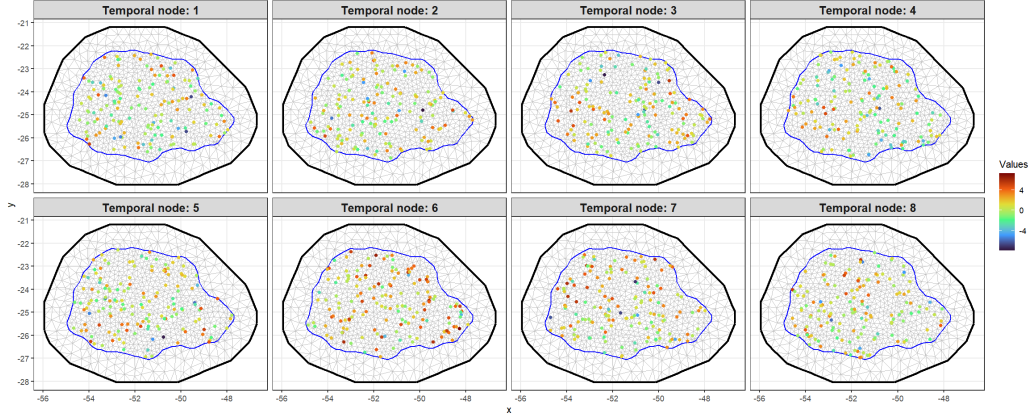


Figure 1: Spatial mesh for the Paraná state and simulated data in the case of $n = 150$ (locations changing randomly in time) and $T = 8$.

terval Width (AIW), calculated separately for the training set (80% of the simulated data) and the test set (20% of the data); the definitions of these metrics are provided in [Appendix B](#). We also present a selection of posterior distributions from the INLA output and from the implementation of INLA-RF1, with and without uncertainty propagation, for the observations with the highest RMSE under the benchmark SPDE model.

Table 1 presents the results obtained for the 80/20 training/testing split (the INLA label is used for the benchmark SPDE model, while INLA-RF1.1 and INLA-RF1.2 refer to the INLA-RF1 algorithm without and with uncertainty propagation, respectively). From this table, we can observe that applying INLA-RF1, regardless of uncertainty propagation, improves the RMSE, MAE, and CP metrics. In particular, the AIW metric suggests that when the hybrid approach is applied without uncertainty propagation (INLA-RF1.1), the predictions are more precise —this is because the mean estimates are more accurate, although the uncertainty from the RF is not propagated to the INLA output. However, when uncertainty is propagated (INLA-RF1.2), the significant improvement in CP is accompanied by a wider predictive distribution, as indicated by a larger AIW, compared to the standard approach without hybrid inference.

Measure	Models		
	INLA	INLA-RF1.1	INLA-RF1.2
RMSE	(1.28, 1.80)	(0.59, 1.00)	(0.60, 1.01)
MAE	(0.97, 1.30)	(0.45, 0.75)	(0.46, 0.76)
CP	(0.68, 0.59)	(0.84, 0.68)	(0.97, 0.88)
AIW	(2.19, 2.45)	(1.49, 1.84)	(2.78, 2.99)

Table 1: Performance metrics using an 80/20 training/testing split. The INLA model corresponds to the base INLA model used as benchmark. INLA-RF1.1 refers to the INLA-RF1 model without uncertainty propagation, while INLA-RF1.2 includes uncertainty propagation. Each metric is reported as (training, test).

Figures 2 and 3 show the selected posterior predictive distributions for the 56 observations with the highest RMSE under the INLA model (i.e., the benchmark INLA approach, represented by the black solid line). The first figure corresponds to the training set, while the second shows results for the test set. In general, these figures illustrate that the posterior distributions (orange dashed lines) obtained using INLA-RF1 algorithm without uncertainty propagation yield better alignment with the true simulated values (corresponding to the vertical lines), though with reduced uncertainty—this is due to not accounting for variability from the RF output. In contrast, when the algorithm is applied with uncertainty propagation (green and dot-dashed), we observe an improvement in the localization of the true values, but at the cost of increased uncertainty (i.e., higher variance) compared to the INLA model.

In [Appendix A](#) we perform a CV analysis to evaluate the model’s performance under a structured spatio-temporal k -fold partitioning ([Roberts et al., 2017](#); [Meyer et al., 2018](#)) in order to take into account the spatio-temporal structure of the data when splitting into training and test. The results show that the average performance, as well as the performance for each individual CV partition, is consistent with the results obtained when using a standard (80% – 20%) training-test split.

3.2. Purely temporal simulation study for INLA-RF2

In this section we provide an example involving a purely temporal application of INLA-RF2 with simulated data. The objective and motivation of this section is to present a particularly simple and visually clear application of the algorithm.

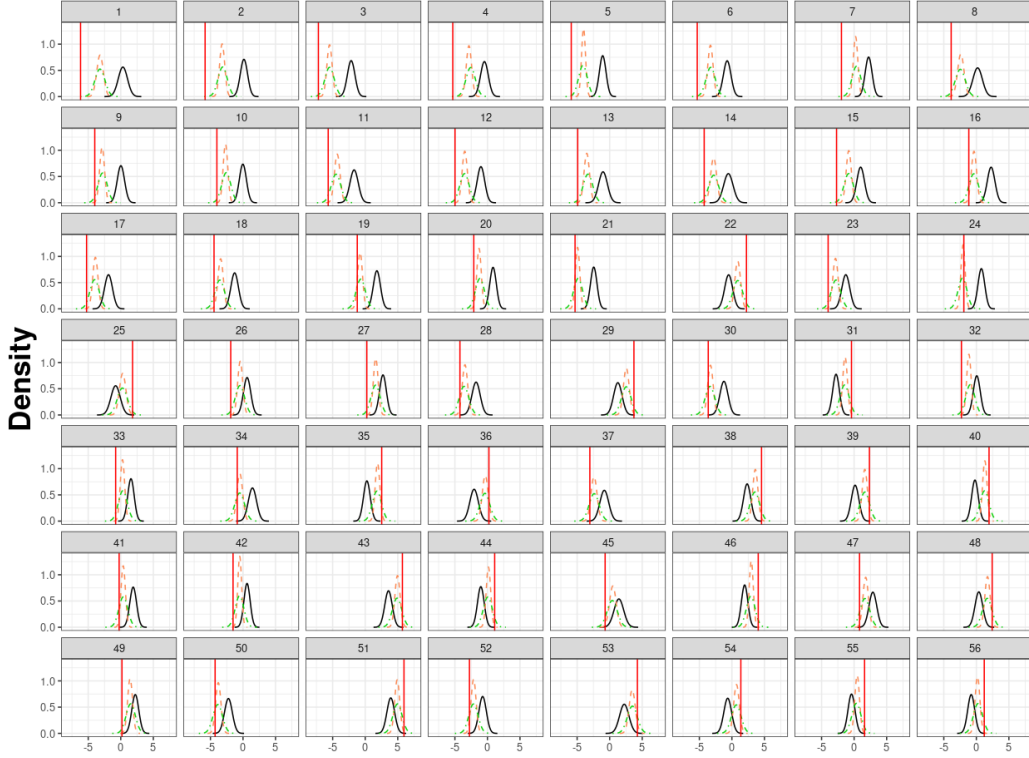


Figure 2: Posterior distributions of the linear predictor for the 56 observations in the training data set with higher RMSE values computed using the benchmark INLA model. The black solid line show the benchmark INLA output, orange dashed and green dot-dashed lines correspond to the output from Algorithm 1 without and with uncertainty propagation, respectively. Red vertical lines indicate the simulated (true) values.

The example is constructed by simulating a time series \mathbf{y} with n time points including a given number of jumps imposed at equally spaced time locations. The simulation model is defined as follows using matrix notation:

$$\begin{aligned} \mathbf{y} &\sim \text{MVN}(\boldsymbol{\mu}, \tau_\ell \mathbf{I}) \\ \boldsymbol{\mu} &= \text{vec}(1)\beta_0 + \mathbf{u}, \end{aligned} \tag{11}$$

where $\text{vec}(\cdot)$ is the vectorization operator, β_0 is the model intercept, and \mathbf{u} is a temporal random effect that incorporates k jumps. In particular, it is defined as:

$$\mathbf{u} = \mathbf{D}\mathbf{w} + \mathbf{u}_r,$$

where \mathbf{D} is a $n \times k$ matrix whose elements identify the time indices at which

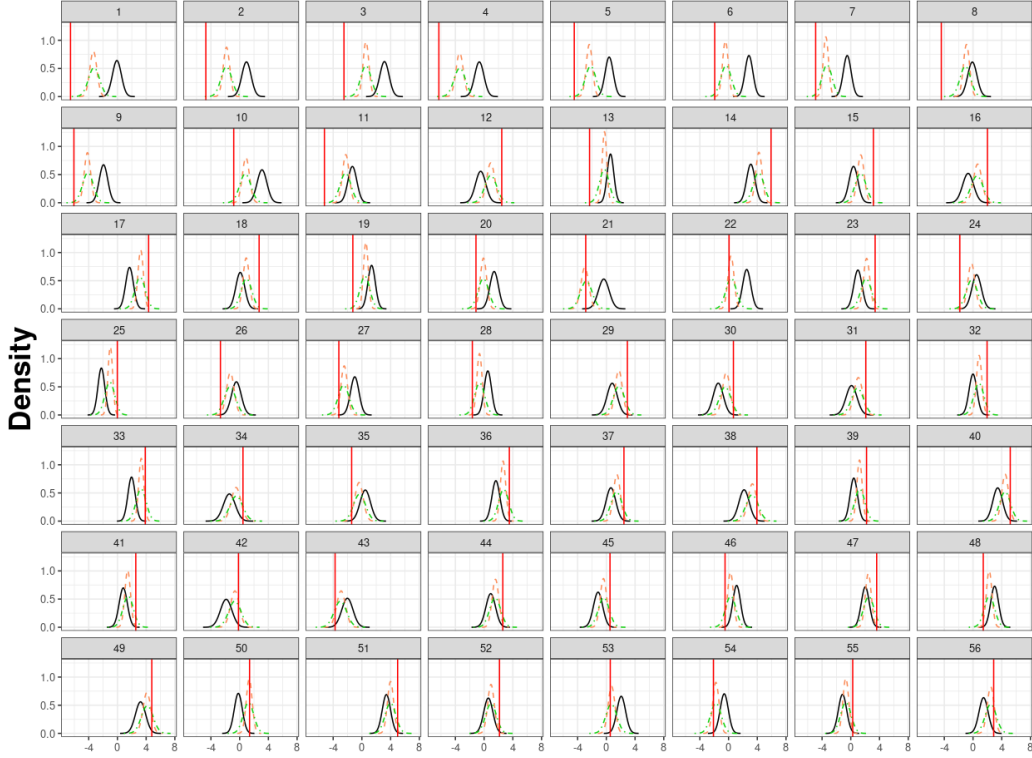


Figure 3: Posterior distributions of the linear predictor for the 56 observations in the test data set with higher RMSE values computed using the benchmark INLA model. The black solid line show the benchmark INLA output, orange dashed and green dot-dashed lines correspond to the output from Algorithm 1 without and with uncertainty propagation, respectively. Red vertical lines indicate the simulated (true) values.

jumps are introduced, and \mathbf{w} is the corresponding k -dimensional vector that defines the jump magnitudes. The jump vector is defined as $\mathbf{w} = \text{sign}(\mathbf{w}_s - 0.5) \cdot \mathbf{w}_j$, with $\mathbf{w}_s \sim \text{Binom}(\boldsymbol{\pi}_s)$ and $\mathbf{w}_j \sim \text{MVN}(\boldsymbol{\mu}_{w_j}, \tau_{w_j} \mathbf{I})$. Finally, \mathbf{u}_r is generated according to a first-order random walk (*RW1*), such that $\Delta \mathbf{u}_r \sim \text{MVN}(\mathbf{0}, \tau_{u_r} \mathbf{I})$, with Δ being the first-order difference operator.

Table 2 displays the parameter values and model components used for the simulation with $n = 2000$ time points, and a matrix \mathbf{D} encoding 10 jumps. Each of the k columns of the matrix \mathbf{D} is defined by elements that corresponds to a vector of dimension 181×1 , except for the last one, which is 190×1 . Therefore, \mathbf{D} acts as a cumulative matrix. The simulated data \mathbf{y} generated from the model structure in Eq. (11) is shown in Figure 4 where

Parameter	Value
β_0	2
$\boldsymbol{\pi}_s$	$\text{vec}(0.5)$
$\boldsymbol{\mu}_{w_j}$	$\text{vec}(5)$
τ_ℓ	20
τ_{w_j}	10
τ_{u_r}	20

$$\mathbf{D} = \begin{bmatrix} \mathbf{0} & \mathbf{0} & \dots & \dots & \dots & \mathbf{0} \\ \mathbf{1} & \mathbf{0} & \vdots & \vdots & \vdots & \mathbf{0} \\ \mathbf{1} & \mathbf{1} & \vdots & \vdots & \vdots & \mathbf{0} \\ \vdots & \vdots & \dots & \mathbf{1} & \vdots & \vdots \\ \mathbf{1} & \mathbf{1} & \dots & \dots & \dots & \mathbf{1} \end{bmatrix}$$

Table 2: Values of the parameters and components used in the simulation.

the temporal trend and the jumps in the time series are visible.

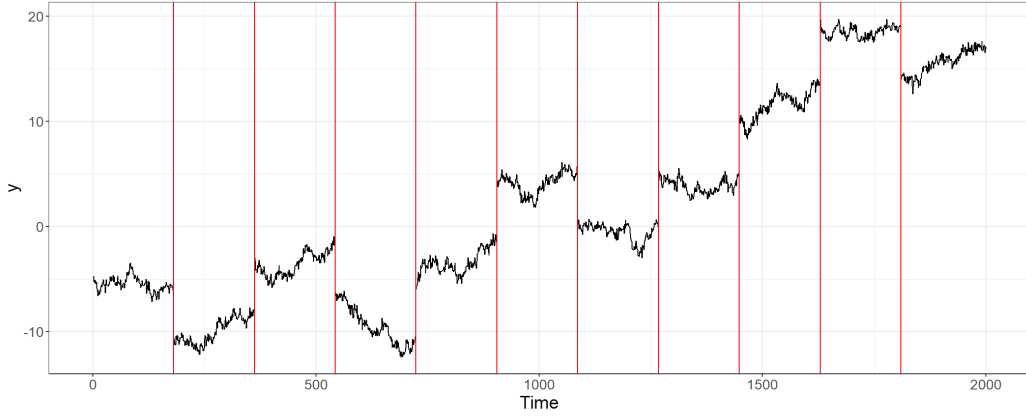


Figure 4: Simulated time series with 2000 time points and 10 jumps (highlighted with red vertical lines).

Once the data have been simulated, the first step for implementing INLA-RF2 consists in defining a base INLA model to define the latent field to be corrected (see State 1 and 2 in Algorithm 2); this model will also be used as benchmark for the comparison. In this case, the INLA base model, which is purely temporal, is defined as follows in matrix form:

$$\mathbf{y} = \text{vec}(1)\beta_0 + \mathbf{u} + \boldsymbol{\varepsilon}_\ell, \quad (12)$$

where β_0 is an intercept and $\boldsymbol{\varepsilon}_\ell \sim \text{MVN}(\mathbf{0}, \tau_\ell)$. The term \mathbf{u} is a second-order random walk process (*RW2*), such that $\Delta^2 \mathbf{u} \sim \text{MVN}(\mathbf{0}, \tau_u \mathbf{I})$. The

results obtained from this model for the temporal random effect and the linear predictor $\boldsymbol{\eta} = \text{vec}(\mathbf{1})\beta_0 + \mathbf{u}$ are shown in Figure 5. Panel A shows the temporal component, with the simulated time series shown as a black line and the posterior mean of the inferred result in blue, along with the 95% Credible Interval (CI) in light blue. Panels B and C show the marginal variance values for each node of the temporal random effect ($\mathbf{u} = (u_1, \dots, u_n)$) and for each node of the linear predictor ($\boldsymbol{\eta} = (\eta_1, \dots, \eta_n)$), respectively. These are shown together with the locations where jumps were introduced, highlighted with vertical red lines. As it can be seen in panels B and C, the highest marginal variance values are associated with the boundary nodes of the model, due to the structure of the precision matrix for the temporal component, and with those nodes located close to where jumps were introduced.

To identify the stress points (i.e., the nodes in the latent field that will be corrected) we selected the 100 nodes of the temporal random effect with the highest marginal variance. The set of nodes to be corrected (stress points) is shown in Figure 6.

Having selected the nodes for correction, we can proceed with the implementation of the hybrid INLA-RF2 model. In particular, the extended model used in STEP 1 of Algorithm 2 includes the new random effects and is defined as:

$$\begin{aligned} \mathbf{y} &\sim \text{MVN}(\boldsymbol{\mu}, \tau_\ell \mathbf{I}) \\ \boldsymbol{\mu} &= \text{vec}(\mathbf{1})\beta_0 + \mathbf{u} + \mathbf{A}_c \mathbf{x}'_c, \end{aligned} \quad (13)$$

where \mathbf{A}_c is a projection matrix that identifies the observations associated with the stress point nodes and integrates the correction values \mathbf{x}'_c into the temporal component at those locations. The component \mathbf{x}'_c represents the values correcting the stress points, and is modeled as $\mathbf{x}'_c \sim \text{MVN}(\boldsymbol{\mu}'_c, \tau'_c \mathbf{I})$, where $\boldsymbol{\mu}'_c$ contains the predictions obtained via RF residual analysis, and τ'_c corresponds to the OOB variance derived from the RF. Both $\boldsymbol{\mu}'_c$ and τ'_c are iteratively updated following Algorithm 2, until the stopping criterion is met.

3.2.1. Results

Figures 7 and 8 present the results of INLA-RF2 when the first KLD criterion is used as stopping criterion (see Eq. (6)). In particular, we compare the corrected latent field—which is the output of INLA-RF2 algorithm—and the original latent field, i.e. estimated using the base INLA model with no RF hybridization. Results are highlighted for some selected stress points.

Figure 7 displays the original time series (in black) together with the posterior mean (and 95% CI) of the corrected and original latent field. Moreover,

zoomed-in views of the areas near the jumps are included to highlight differences. It can be seen that in areas near the imposed jumps, the corrected latent field provides a better estimate than the original.

Figure 8 illustrates the effect of correcting the stress points using INLA-RF2. Specifically, it compares the latent field estimates for the 100 stress points between the original INLA model (black dots and bars for the posterior mean 95% CI, respectively) and from the INLA-RF2 hybrid model (red dots and bars). The true simulated values are shown as blue horizontal lines. An overall improvement in the latent field estimates can be seen after applying the latent field nodes correction via INLA-RF2. In fact, the corrected estimates (in red) align more closely with the true values, while the base INLA model (in black) shows noticeable bias, especially in time points characterized by a rapid change of level. These results highlight the ability of the INLA-RF2 hybrid model to effectively correct the latent field in targeted regions.

Table 3 presents the performance measures for both the full dataset and the subset corresponding to stress points when comparing INLA-RF2 against the INLA base model. The INLA-RF2 approach demonstrates clear improvements in accuracy, especially at the stress points, where the RMSE decreases substantially from 0.93 (INLA) to 0.22 (INLA-RF2), and MAE from 0.65 to 0.13. Additionally, INLA-RF2 shows improved uncertainty quantification at stress points, as indicated by CP and AIW.

Models		
Measure	INLA	INLA-RF2
RMSE	(0.34, 0.93)	(0.27, 0.22)
MAE	(0.22, 0.65)	(0.20, 0.13)
CP	(0.83, 0.47)	(0.70, 0.92)
AIW	(0.69, 0.71)	(0.52, 0.92)

Table 3: Performance metrics for the INLA-RF2 algorithm and the INLA base model, reported for the full dataset and for the subset corresponding to stress points (full dataset, stress points).

4. Discussion and conclusion

In this paper, we proposed two algorithms —INLA-RF1 and INLA-RF2— for performing hybrid inference by combining a base INLA model —which

can include spatial, temporal and spatio-temporal random effects— with RF. These two algorithms differ in their objectives: while the first is designed to correct the model offset, the second focuses on correcting specific nodes of the latent field, providing localized improvements in model estimates. This can also be interpreted as a correction applied over a reduced subset of the graph of the latent GMRF model. The first algorithm is relatively straightforward to implement and apply, whereas the second requires the user to define a set of nodes to be corrected using RF. This adds a layer of complexity, as it requires precise knowledge of which nodes should be modified for the algorithm’s application to be meaningful.

We choose to apply the INLA-SPDE model as the first stage of our hybrid strategy in order to capture structured, interpretable spatio-temporal effects and covariate relationships within a fully Bayesian framework. This allows us to obtain posterior distributions for both parameters and latent fields, which serve as a coherent foundation for downstream corrections. The RF is then applied to the residuals, which contain the remaining non-linear and local variation not captured by the parametric model.

For INLA-RF1, the final output is obtained by combining the predictions from the last INLA model run with the RF correction, which can be performed either with or without uncertainty propagation. In contrast, INLA-RF2 directly incorporates the RF correction into the latent field nodes during the final INLA run. This approach ensures that the algorithm concludes with the Bayesian INLA model, providing full posterior distributions. It effectively integrates the RF correction while simultaneously propagating the associated uncertainty, quantified via the RF OOB variance.

Both hybrid strategies exploits the computational advantages given by the INLA-SPDE approach. To reduce the computational cost given by the iterative process of the INLA-RF algorithms, we leverage the fact that the modal configuration of the hyperparameters $\boldsymbol{\theta}$ obtained in previous steps is typically close to the mode in subsequent steps. By providing these previous estimates as initial values to the `inla` function, the optimization algorithm can locate faster the mode of the marginal posterior $\pi(\boldsymbol{\theta} \mid \mathbf{y})$. This reuse of information significantly reduces the computational cost associated with mode-finding in each iteration.

A key component of the INLA-RF algorithms is the stopping criterion we introduce, which is based on a divergence measure, the Kullback-Leibler divergence, a widely used measure of cross-entropy. While other divergence measures could be considered, the KL divergence is particularly attractive

in our setting because it admits analytical expressions for Gaussian distributions, making it a highly efficient choice for quickly evaluating the divergence between two Gaussian probability densities. This stopping criterion allows us to assess convergence of the iterative hybrid procedure, ensuring that the contributions of each model component stabilize over iterations. Importantly, it is not treated as a tuning parameter as in [MacBride et al. \(2025\)](#), and this enhances the objectivity of the procedure and reduces the risk of overfitting or unnecessary repeated runs.

In the simulation studies presented in this paper, our INLA-RF algorithms consistently outperformed the base INLA model —i.e., with no hybridization— in terms of both predictive accuracy and uncertainty quantification. The modular nature of the INLA-RF framework makes it highly adaptable and well-suited for extensions. For instance, alternative machine learning or deep learning models could be used in place of Random Forests. Moreover, non-Gaussian likelihoods or other random effects could be incorporated in the first parametric modeling step to handle more complex data structures.

Author Contributions

The authors (Mario Figueira = MF, Michela Cameletti = MC, Luca Patelli = LP) contributed to the paper as follows:

- Conceptualization: MC, MF, LP
- Methodology: MC, MF
- Code: MF, LP
- Formal data analysis: MF
- Writing – original draft: MC, MF, LP
- Writing – review & editing: MC, MF, LP
- Supervision: MC

Funding

MF acknowledges support from Grant PID2022-136455NB-I00, funded by Ministerio de Ciencia, Innovación y Universidades of Spain (MCIN/AEI/10.13039/501100011033/FEDER, UE) and the European Regional Development Fund.

Code and data availability

The code for generating the data for the two simulation studies, as well as for implementing the proposed methodologies, is publicly available on GitHub in the following repository: <https://github.com/LucaPate/SPDE-Forest/tree/main>.

Declaration of generative AI and AI-assisted technologies in the writing process

During the preparation of this work the authors used [OpenAI \(2025\)](#) in order to improve the readability and language of the manuscript. After using this tool, the authors reviewed and edited the content as needed and take full responsibility for the content of the published article.

References

- N. Cressie, C. K. Wikle, Statistics for Spatio-Temporal data, Wiley, 2011.
- E. T. Krainski, V. Gómez-Rubio, H. Bakka, A. Lenzi, D. Castro-Camilo, D. Simpson, F. Lindgren, H. Rue, Advanced Spatial Modeling with Stochastic Partial Differential Equations Using R and INLA, CRC-Press, 2018.
- C. K. Wikle, A. Zammit-Mangion, N. Cressie, Spatio-Temporal Statistics with R, CRC-Press, 2019.
- H. Rue, S. Martino, N. Chopin, Approximate Bayesian inference for latent Gaussian models by using integrated nested Laplace approximations, Journal of the Royal Statistical Society. Series B: Statistical Methodology 71 (2009) 319–392. doi:[10.1111/j.1467-9868.2008.00700.x](https://doi.org/10.1111/j.1467-9868.2008.00700.x).
- F. Lindgren, H. Rue, J. Lindström, An explicit link between Gaussian Fields and Gaussian Markov Random Fields: the Stochastic Partial Differential Equation approach, J. Royal Stat. Soc.: Series B (Statistical Methodology) 73 (2011) 423–498.
- M. Pichler, F. Hartig, Machine learning and deep learning—a review for ecologists, Methods in Ecology and Evolution 14 (2023) 994–1016. doi:<https://doi.org/10.1111/2041-210X.14061>.

- C. K. Wikle, A. Zammit-Mangion, Statistical deep learning for spatial and spatiotemporal data, *Annual Review of Statistics and Its Application* 10 (2023) 247–270.
- I. E. Agbehadji, I. C. Obagbuwa, Systematic review of machine learning and deep learning techniques for spatiotemporal air quality prediction, *Atmosphere* 15 (2024).
- E. W. Fox, J. M. Ver Hoef, A. R. Olsen, Comparing spatial regression to random forests for large environmental data sets, *PLoS One* 15 (2020) e0229509.
- P. S. G. de Mattos Neto, G. D. C. Cavalcanti, D. S. de O. Santos Júnior, J. A. de Souza, F. Ren, Hybrid systems using residual modeling for sea surface temperature forecasting, *Scientific Reports* 12 (2022) 487. URL: <https://doi.org/10.1038/s41598-021-04238-z>. doi:10.1038/s41598-021-04238-z.
- D. P. Johnson, N. Ravi, G. Filippelli, A. Heintzelman, A Novel Hybrid Approach: Integrating Bayesian SPDE and Deep Learning for Enhanced Spatiotemporal Modeling of PM_{2.5} Concentrations in Urban Airsheds for Sustainable Climate Action and Public Health, *Sustainability* 16 (2024). URL: <https://www.mdpi.com/2071-1050/16/23/10206>.
- A. Kakouri, T. Kontos, G. Grivas, G. Filippis, M.-B. Korrás-Carraca, C. Matsoukas, A. Gkikas, E. Athanasopoulou, O. Speyer, C. Chatzidiakos, E. Gerasopoulos, Spatiotemporal modeling of long-term PM_{2.5} concentrations and population exposure in Greece, using machine learning and statistical methods, *Science of The Total Environment* 958 (2025) 178113. doi:<https://doi.org/10.1016/j.scitotenv.2024.178113>.
- Q. Di, H. Amini, L. Shi, I. Kloog, R. Silvern, J. T. Kelly, M. B. Sabath, C. Choirat, P. Koutrakis, A. Lyapustin, et al., An ensemble-based model of PM_{2.5} concentration across the contiguous United States with high spatiotemporal resolution, *Environment International* 130 (2019) 104909.
- I. A. Gheys, L. S. Smith, A novel neural network ensemble architecture for time series forecasting, *Neurocomputing* 74 (2011) 3855–3864. doi:<https://doi.org/10.1016/j.neucom.2011.08.005>.

- F. Saad, J. Burnim, C. Carroll, et al., Scalable spatiotemporal prediction with bayesian neural fields, *Nature Communications* 15 (2024) 7942. URL: <https://doi.org/10.1038/s41467-024-51477-5>. doi:10.1038/s41467-024-51477-5.
- C. MacBride, V. Davies, D. Lee, A spatial autoregressive random forest algorithm for small-area spatial prediction, *The Annals of Applied Statistics* 19 (2025) 485 – 504. doi:10.1214/24-A0AS1969.
- G. Jona Lasinio, G. Mastrantonio, A. Pollice, Discussing the “big n problem”, *Statistical Methods and Applications* 22 (2013) 97–112. URL: <https://doi.org/10.1007/s10260-012-0207-2>. doi:10.1007/s10260-012-0207-2.
- F. Lindgren, D. Bolin, H. Rue, The SPDE approach for Gaussian and non-Gaussian fields: 10 years and still running, *Spatial Statistics* 50 (2022). doi:<https://doi.org/10.1016/j.spasta.2022.100599>, special Issue: The Impact of Spatial Statistics.
- F. Lindgren, H. Rue, Bayesian Spatial Modelling with R-INLA, *Journal of Statistical Software* 63 (2015) 1–25. doi:10.18637/jss.v063.i19.
- H. Bakka, H. Rue, G.-A. Fuglstad, A. Riebler, D. Bolin, J. Illian, E. Krainski, D. Simpson, F. Lindgren, Spatial modeling with r-inla: A review, *WIREs Computational Statistics* 10 (2018) e1443. doi:<https://doi.org/10.1002/wics.1443>.
- V. Gómez-Rubio, *Bayesian Inference with INLA*, Chapman & Hall/CRC Press, 2020. doi:10.1201/9781315175584.
- J. Van Niekerk, H. Rue, Low-rank Variational Bayes correction to the Laplace method, *Journal of Machine Learning Research* 25 (2024) 1–25.
- J. Van Niekerk, E. Krainski, D. Rustand, H. Rue, A new avenue for Bayesian inference with INLA, *Computational Statistics & Data Analysis* 181 (2023) 107692. doi:10.1016/j.csda.2023.107692.
- H. Rue, L. Held, *Gaussian Markov Random Fields*, Chapman and Hall/CRC, 2005. doi:10.1201/9780203492024.

- F. Lindgren, H. Rue, J. Lindström, An explicit link between Gaussian fields and Gaussian Markov random fields: the stochastic partial differential equation approach, *Journal of the Royal Statistical Society: Series B (Statistical Methodology)* 73 (2011) 423–498. doi:<https://doi.org/10.1111/j.1467-9868.2011.00777.x>.
- L. Breiman, Random forests, *Machine learning* 45 (2001) 5–32.
- B. Efron, Bootstrap Methods: Another Look at the Jackknife, *The Annals of Statistics* 7 (1979) 1 – 26. URL: <https://doi.org/10.1214/aos/1176344552>. doi:10.1214/aos/1176344552.
- L. Breiman, J. Friedman, C. J. Stone, R. Olshen, *Classification and regression tree analysis*, CRC Press, 1984.
- G. James, D. Witten, T. Hastie, R. Tibshirani, *An Introduction to Statistical Learning: with Applications in R*, 2nd ed., Springer US, 2021.
- L. Patelli, M. Cameletti, N. Golini, R. Ignaccolo, A Path in Regression Random Forest Looking for Spatial Dependence: A Taxonomy and a Systematic Review, *Springer Nature Switzerland, Cham*, 2024, pp. 467–489. doi:10.1007/978-3-031-69111-9_23.
- A. Saha, S. Basu, A. Datta, Random forests for spatially dependent data, *Journal of the American Statistical Association* 118 (2023) 665–683.
- M. J. Heaton, A. Millane, J. S. Rhodes, Adjusting for spatial correlation in machine and deep learning, 2024. URL: <https://arxiv.org/abs/2410.04312>. arXiv:2410.04312.
- S. Kullback, *Information Theory and Statistics*, A Wiley publication in mathematical statistics, Dover Publications, 1997.
- M. Cameletti, F. Lindgren, D. Simpson, H. Rue, Spatio-temporal modeling of particulate matter concentration through the SPDE approach, *AStA Advances in Statistical Analysis* 97 (2013) 109–131. URL: <https://doi.org/10.1007/s10182-012-0196-3>. doi:10.1007/s10182-012-0196-3.
- P. Moraga, *Geospatial Health Data: Modeling and Visualization with R-INLA and Shiny*, Chapman & Hall/CRC, 2019.

- G. Fioravanti, S. Martino, M. Cameletti, G. Cattani, Spatio-temporal modelling of PM10 daily concentrations in Italy using the SPDE approach, *Atmospheric Environment* 248 (2021) 118192.
- G. Fioravanti, M. Cameletti, S. Martino, G. Cattani, E. Pisoni, A spatiotemporal analysis of NO concentrations during the Italian 2020 COVID-19 lockdown, *Environmetrics* 33 (2022) e2723.
- G. Fioravanti, S. Martino, M. Cameletti, A. Toreti, Interpolating climate variables by using INLA and the SPDE approach, *International Journal of Climatology* 43 (2023) 6866–6886.
- P. Otto, A. F. Moro, J. Rodeschini, Q. Shaboviq, R. Ignaccolo, N. Golini, M. Cameletti, P. Maranzano, F. Finazzi, A. Fassò, Spatiotemporal modelling of PM_{2.5} concentrations in Lombardy (Italy): a comparative study, *Environmental and Ecological Statistics* 31 (2024) 245–272. doi:[10.1007/s10651-023-00589-0](https://doi.org/10.1007/s10651-023-00589-0).
- D. Simpson, H. Rue, A. Riebler, T. G. Martins, S. H. Sørbye, Penalising model component complexity: A principled, practical approach to constructing priors, *Statistical Science* 32 (2017) 1–28. doi:[10.1214/16-STS576](https://doi.org/10.1214/16-STS576).
- G.-A. Fuglstad, D. Simpson, F. Lindgren, H. Rue, Constructing Priors that Penalize the Complexity of Gaussian Random Fields, *Journal of the American Statistical Association* 114 (2019) 445–452. doi:[10.1080/01621459.2017.1415907](https://doi.org/10.1080/01621459.2017.1415907).
- D. R. Roberts, V. Bahn, S. Ciuti, M. S. Boyce, J. Elith, G. Guillerá-Arroita, S. Hauenstein, J. J. Lahoz-Monfort, B. Schröder, W. Thuiller, D. I. Warton, B. A. Wintle, F. Hartig, C. F. Dormann, Cross-validation strategies for data with temporal, spatial, hierarchical, or phylogenetic structure, *Ecography* 40 (2017) 913–929. doi:[10.1111/ecog.02881](https://doi.org/10.1111/ecog.02881), publisher: Wiley.
- H. Meyer, C. Reudenbach, T. Hengl, M. Katurji, T. Nauss, Improving performance of spatio-temporal machine learning models using forward feature selection and target-oriented validation, *Environmental Modelling & Software* 101 (2018) 1–9. doi:[10.1016/j.envsoft.2017.12.001](https://doi.org/10.1016/j.envsoft.2017.12.001), publisher: Elsevier BV.

OpenAI, Chatgpt (gpt-4-turbo, accessed june 2025), <https://chat.openai.com>, 2025. Large language model.

Appendix A. Spatio-temporal simulation study for INLA-RF1: Cross-Validation results

In this section we propose a Cross-Validation (CV) analysis for the spatio-temporal simulation study for INLA-RF1 (see Section 3.1 of the main manuscript). The aim is to evaluate the model’s performance under a structured spatio-temporal k -fold partitioning in order to take into account the spatio-temporal structure of the data when splitting into training and test. The procedure used to construct the spatio-temporal blocks (or clusters) can be summarized as follows: first, the temporal nodes to be aggregated are selected. For each temporal aggregation, a fixed spatial partitioning of the data using the k -means algorithm is applied using the spatial coordinates of the observations. This results in a spatio-temporal partition where the overall dimensionality is determined by the number of aggregated temporal nodes and the number of centroids specified in the k -means algorithm. For the CV analysis, one of the partitions is selected as the test set, and the remaining partitions are used as the training set. For example, if the data is divided into six spatio-temporal partitions, one partition is used for testing purposes and the remaining partitions serve as the training set. This process is then repeated until all the partitions have been used as the test set. As a result, we obtain performance metrics for each partition, which can then be averaged to compute an overall performance estimate. Figure A.9 shows the six spatio-temporal clusters along with the data assigned to each of them. The results related to the case with 8 and 16 blocks are presented later.

Table A.4 shows that the average performance, as well as the performance for each individual partition, is consistent with the results obtained when using a standard (80% – 20%) training-test split. Specifically, applying INLA-RF1 improves the identification of true values. The most precise predictions are obtained when uncertainty from the RF component is not propagated to the INLA model, as expected. When uncertainty is propagated, the predictive intervals become wider than in the benchmark approach. Nevertheless, both versions of INLA-RF1 - whether uncertainty is propagated or not - lead to lower estimation error and better coverage of the true values, although the version with uncertainty propagation results in wider intervals compared to the benchmark method.

We now report the results of the CV analysis when using 8 and 16 spatio-temporal blocks.

Figure A.10 shows the spatio-temporal clustering of the observations for

<i>Blocks</i>						
Model	1	2	3	4	5	6
RMSE						
INLA	(1.35, 1.90)	(1.37, 1.82)	(1.39, 1.69)	(1.39, 1.58)	(1.33, 1.91)	(1.38, 1.57)
INLA-RF1.1	(0.62, 1.20)	(0.61, 1.21)	(0.63, 1.21)	(0.62, 1.07)	(0.63, 1.27)	(0.61, 1.04)
INLA-RF1.2	(0.62, 1.22)	(0.62, 1.19)	(0.64, 1.17)	(0.62, 1.08)	(0.62, 1.29)	(0.61, 1.05)
MAE						
INLA	(1.01, 1.45)	(1.01, 1.36)	(1.03, 1.29)	(1.03, 1.20)	(0.99, 1.45)	(1.03, 1.14)
INLA-RF1.1	(0.46, 0.92)	(0.46, 0.91)	(0.48, 0.93)	(0.47, 0.85)	(0.47, 1.03)	(0.48, 0.79)
INLA-RF1.2	(0.47, 0.94)	(0.46, 0.90)	(0.48, 0.9)	(0.47, 0.85)	(0.47, 1.04)	(0.48, 0.79)
CP						
INLA	(0.62, 0.65)	(0.62, 0.68)	(0.62, 0.74)	(0.64, 0.74)	(0.65, 0.65)	(0.65, 0.76)
INLA-RF1.1	(0.77, 0.72)	(0.78, 0.76)	(0.76, 0.75)	(0.78, 0.78)	(0.77, 0.77)	(0.78, 0.86)
INLA-RF1.2	(0.98, 0.85)	(0.97, 0.88)	(0.97, 0.90)	(0.97, 0.94)	(0.97, 0.91)	(0.97, 0.95)
AIW						
INLA	(2.05, 3.05)	(2.03, 3.16)	(2.12, 3.33)	(2.14, 3.50)	(2.13, 3.26)	(2.19, 3.32)
INLA-RF1.1	(1.34, 2.56)	(1.31, 2.64)	(1.36, 2.87)	(1.35, 2.82)	(1.38, 2.78)	(1.37, 2.64)
INLA-RF1.2	(2.8, 3.57)	(2.76, 3.56)	(2.87, 3.81)	(2.79, 3.77)	(2.82, 3.76)	(2.78, 3.63)

Table A.4: Predictive performance and uncertainty quantification metrics for each model by data set (train, test) under a spatio-temporal partition with 6 clusters or blocks. INLA stands for the standard INLA and SPDE approach; INLA-RF1.1 refers to the implementation of Algorithm 1 without uncertainty propagation and INLA-RF1.2 includes uncertainty propagation.

the cases with 8 and 16 spatio-temporal blocks. The aggregated nodes for each block are indicated in the title of each plot, and the spatial partitions shown correspond to the observations (from the full dataset) assigned to each spatio-temporal block.

Table A.5-A.12 present the CV results for the 8 spatio-temporal block case, using the previously defined metrics: RMSE, MAE, CP, and AIW. In the tables, the INLA label is used for the benchmark INLA model, while INLA-RF1.1 and INLA-RF1.2 refer to Algorithm 1 without and with uncertainty propagation, respectively. Table A.13 shows the average performance indexes values computed across the 8 partitions. Table A.14-A.29 and Table A.30 refer to the case with 16 spatio-temporal blocks.

Block 1		Models	
Measure	INLA	INLA-RF1.1	INLA-RF1.2
RMSE	(1.36, 1.92)	(0.61, 1.29)	(0.61, 1.31)
MAE	(1.01, 1.54)	(0.46, 0.99)	(0.46, 1.00)
CP	(0.63, 0.63)	(0.79, 0.73)	(0.97, 0.83)
AIW	(2.09, 3.22)	(1.36, 2.73)	(2.77, 3.63)

Table A.5: Performance measures for each model by data set (train, test) when Block 1 (out of 8 spatio-temporal blocks) is left out as test set.

Block 2		Models	
Measure	INLA	INLA-RF1.1	INLA-RF1.2
RMSE	(1.37, 1.74)	(0.61, 1.08)	(0.62, 1.07)
MAE	(1.02, 1.29)	(0.46, 0.86)	(0.47, 0.86)
CP	(0.62, 0.73)	(0.77, 0.75)	(0.97, 0.92)
AIW	(2.06, 3.02)	(1.36, 2.59)	(2.8, 3.53)

Table A.6: Performance measures for each model by data set (train, test) when Block 2 (out of 8 spatio-temporal blocks) is left out as test set.

Block 3		Models	
Measure	INLA	INLA-RF1.1	INLA-RF1.2
RMSE	(1.39, 1.86)	(0.61, 1.22)	(0.76, 1.26)
MAE	(1.02, 1.41)	(0.45, 0.91)	(0.58, 0.99)
CP	(0.60, 0.63)	(0.78, 0.75)	(0.97, 0.84)
AIW	(1.98, 2.96)	(1.33, 2.58)	(3.33, 3.59)

Table A.7: Performance measures for each model by data set (train, test) when Block 3 (out of 8 spatio-temporal blocks) is left out as test set.

Block 4		Models	
Measure	INLA	INLA-RF1.1	INLA-RF1.2
RMSE	(1.36, 1.75)	(0.63, 1.18)	(0.63, 1.15)
MAE	(1.01, 1.36)	(0.47, 0.9)	(0.47, 0.89)
CP	(0.63, 0.70)	(0.78, 0.78)	(0.97, 0.92)
AIW	(2.16, 3.38)	(1.37, 2.78)	(2.86, 3.77)

Table A.8: Performance measures for each model by data set (train, test) when Block 4 (out of 8 spatio-temporal blocks) is left out as test set.

Block 5		Models	
Measure	INLA	INLA-RF1.1	INLA-RF1.2
RMSE	(1.42, 1.44)	(0.62, 1.03)	(0.62, 1.02)
MAE	(1.05, 1.11)	(0.48, 0.81)	(0.48, 0.8)
CP	(0.63, 0.78)	(0.75, 0.8)	(0.97, 0.96)
AIW	(2.13, 3.33)	(1.32, 2.65)	(2.78, 3.62)

Table A.9: Performance measures for each model by data set (train, test) when Block 5 (out of 8 spatio-temporal blocks) is left out as test set.

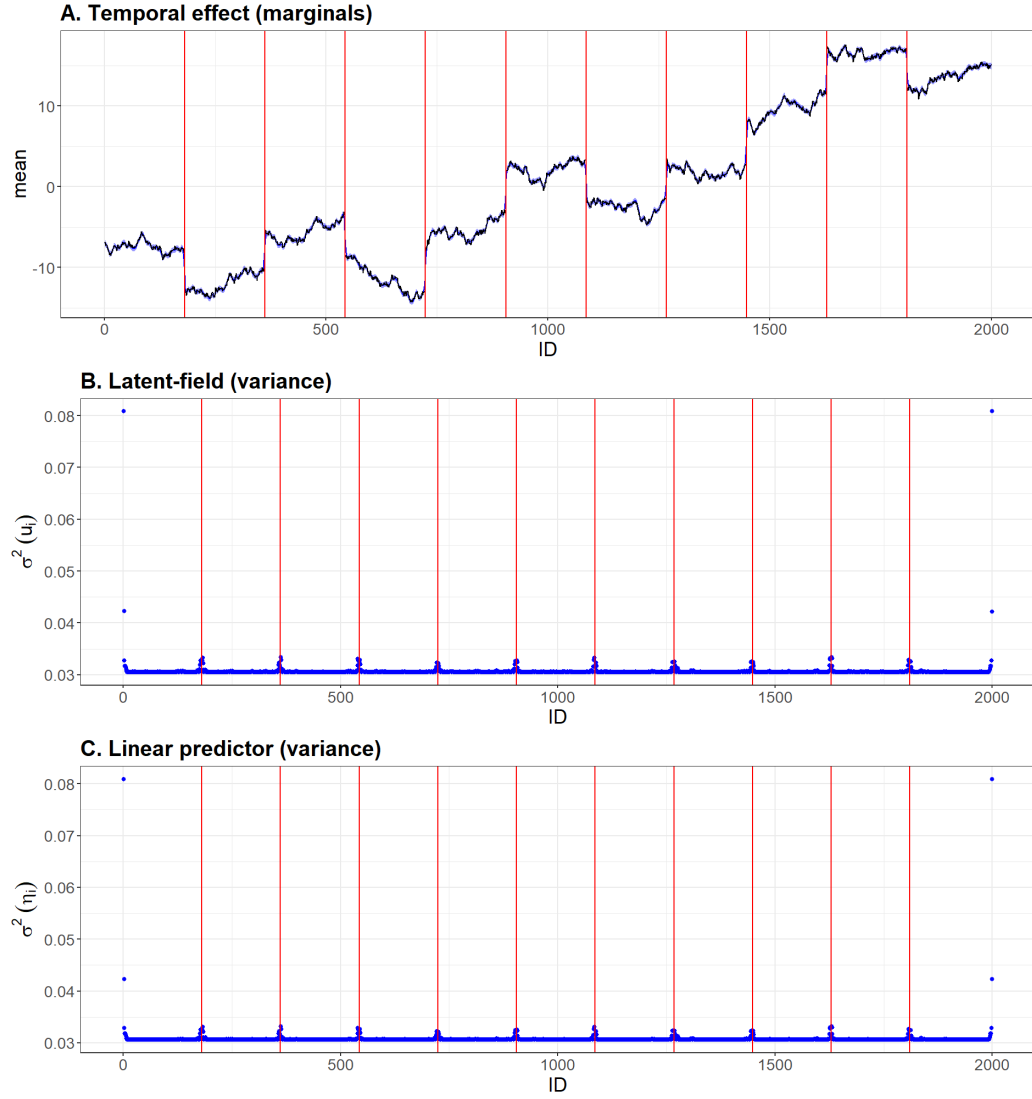


Figure 5: Results from the INLA base model: Panel A shows the temporal random effect, with the simulated time series in black and the posterior mean in blue. The 95% CI is shaded in light blue. Panel B displays the marginal variance of the latent field. Panel C shows the marginal variance of the linear predictor. In all the panels the vertical red lines indicate the locations where jumps were introduced in the simulated data.

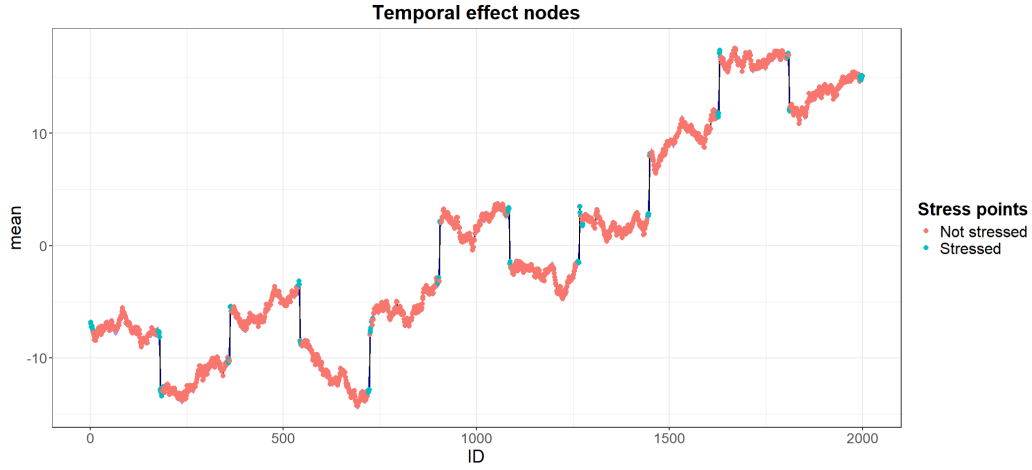


Figure 6: Nodes of the temporal random effect identified as stress points to be corrected, as well as those not considered as stress points according to the highest marginal variance criterion.

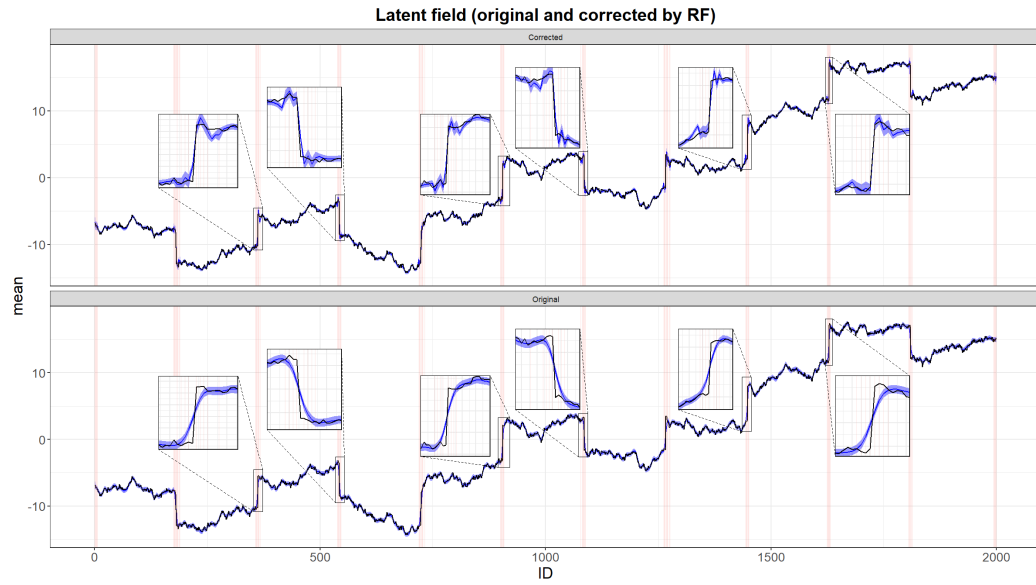


Figure 7: Comparison between the corrected latent field from the INLA-RF2 model (top) and the original latent field from the benchmark INLA model (bottom). In blue, we show the posterior mean with the 95% CI for both the original and corrected models, and in black, the simulated temporal trend. The vertical lines indicate the locations of the 100 stress points.

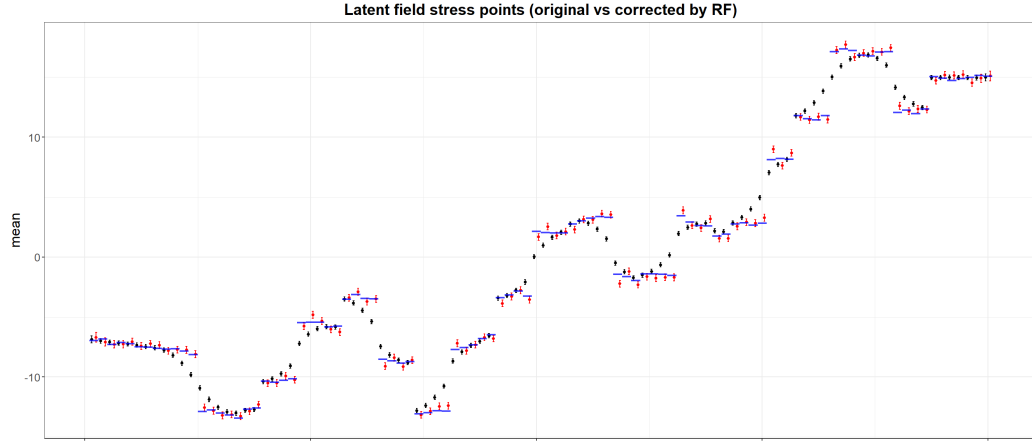


Figure 8: Latent field values at the 100 stress points, comparing the corrected estimates (from INLA-RF2) and the original estimates (from the INLA base model) with the true simulated values. The posterior mean and 95% CI from the base model are shown in black, while the mean and CI shown in red are related to the stress points corrected via Algorithm 2. The true simulated values are displayed using horizontal blue lines.

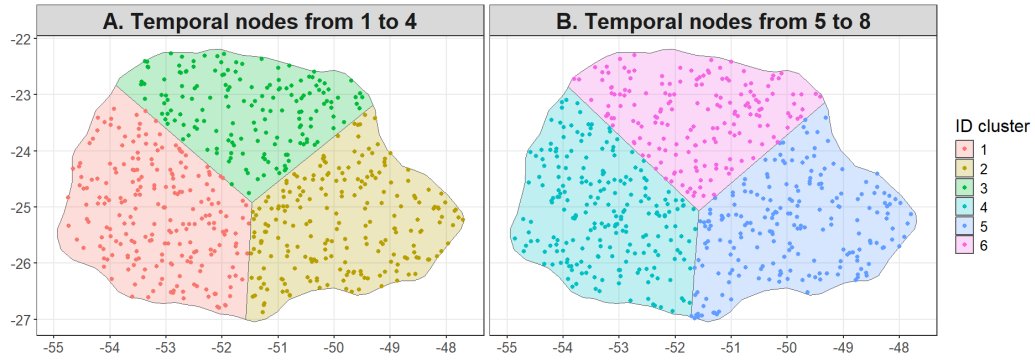
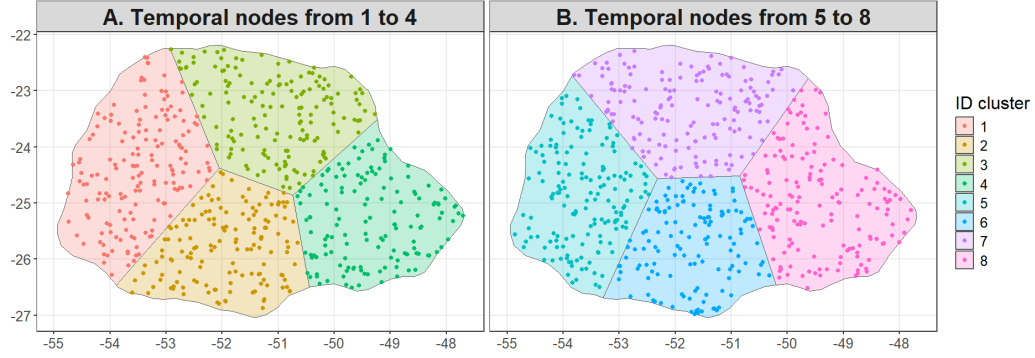
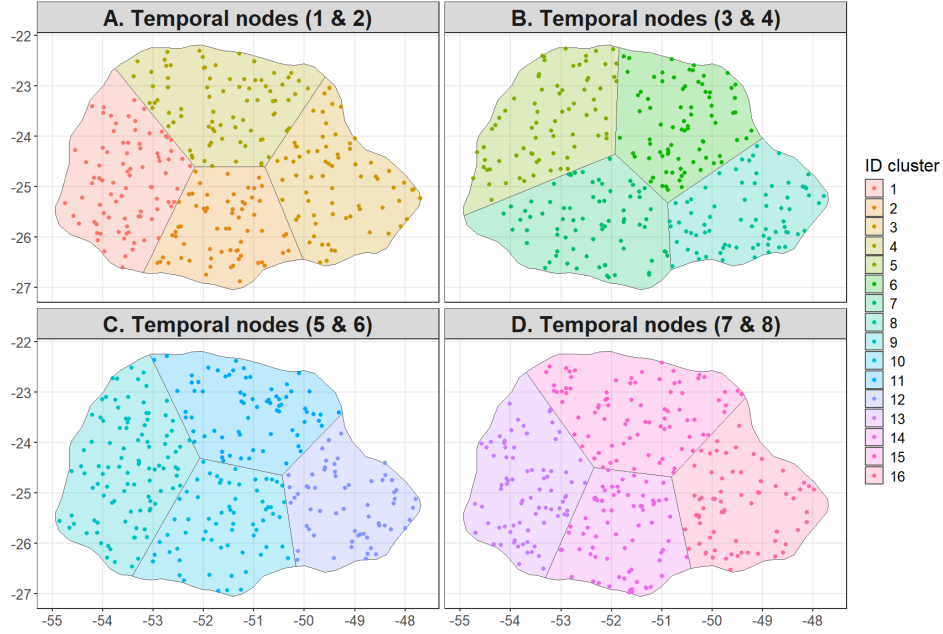


Figure A.9: Spatio-temporal clustering with 6 spatio-temporal blocks, showing the data related to each partition.



(a) Spatio-temporal clustering with 8 spatio-temporal blocks, showing the data related to each partition.



(b) Spatio-temporal clustering with 16 spatio-temporal blocks, showing the data related to each partition.

Figure A.10: Spatio-temporal blocks used for partitioning the data in a spatially and temporally *structured k-fold* cross-validation.

Block 6	Models		
Measure	INLA	INLA-RF1.1	INLA-RF1.2
RMSE	(1.39, 1.41)	(0.62, 0.86)	(0.62, 0.83)
MAE	(1.02, 1.11)	(0.47, 0.71)	(0.47, 0.69)
CP	(0.65, 0.71)	(0.78, 0.84)	(0.97, 0.98)
AIW	(2.17, 3.14)	(1.38, 2.55)	(2.81, 3.55)

Table A.10: Performance measures for each model by data set (train, test) when Block 6 (out of 8 spatio-temporal blocks) is left out as test set.

Block 7	Models		
Measure	INLA	INLA-RF1.1	INLA-RF1.2
RMSE	(1.34, 1.73)	(0.6, 1.16)	(0.6, 1.17)
MAE	(1.00, 1.26)	(0.46, 0.92)	(0.46, 0.92)
CP	(0.65, 0.72)	(0.8, 0.8)	(0.97, 0.87)
AIW	(2.18, 3.48)	(1.36, 2.76)	(2.76, 3.7)

Table A.11: Performance measures for each model by data set (train, test) when Block 7 (out of 8 spatio-temporal blocks) is left out as test set.

Block 8	Models		
Measure	INLA	INLA-RF1.1	INLA-RF1.2
RMSE	(1.34, 2.04)	(0.62, 1.23)	(0.62, 1.26)
MAE	(0.99, 1.50)	(0.46, 0.95)	(0.46, 0.97)
CP	(0.63, 0.64)	(0.76, 0.79)	(0.97, 0.91)
AIW	(2.07, 3.18)	(1.36, 2.75)	(2.80, 3.69)

Table A.12: Performance measures for each model by data set (train, test) when Block 8 (out of 8 spatio-temporal blocks) is left out as test set.

Mean		Models	
Measure	INLA	INLA-RF1.1	INLA-RF1.2
RMSE	(1.37, 1.74)	(0.61, 1.13)	(0.64, 1.14)
MAE	(1.02, 1.32)	(0.46, 0.88)	(0.48, 0.89)
CP	(0.63, 0.69)	(0.78, 0.78)	(0.97, 0.90)
AIW	(2.11, 3.21)	(1.35, 2.67)	(2.86, 3.64)

Table A.13: Performance measures for each model by data set (train, test) across the 8 spatio-temporal blocks.

Block 1		Models	
Measure	INLA	INLA-RF1.1	INLA-RF1.2
RMSE	(1.36, 1.84)	(0.60, 1.23)	(0.61, 1.2)
MAE	(1.01, 1.53)	(0.46, 0.97)	(0.46, 0.95)
CP	(0.63, 0.62)	(0.78, 0.71)	(0.97, 0.87)
AIW	(2.09, 3.24)	(1.34, 2.72)	(2.74, 3.59)

Table A.14: Performance measures for each model by data set (train, test) when Block 1 (out of 16 spatio-temporal blocks) is left out as test set.

Block 2		Models	
Measure	INLA	INLA-RF1.1	INLA-RF1.2
RMSE	(1.39, 1.83)	(0.6, 0.93)	(0.62, 0.92)
MAE	(1.03, 1.44)	(0.45, 0.72)	(0.47, 0.70)
CP	(0.60, 0.55)	(0.79, 0.81)	(0.97, 0.91)
AIW	(2.00, 2.81)	(1.35, 2.44)	(2.77, 3.39)

Table A.15: Performance measures for each model by data set (train, test) when Block 2 (out of 16 spatio-temporal blocks) is left out as test set.

Block 3		Models	
Measure	INLA	INLA-RF1.1	INLA-RF1.2
RMSE	(1.35, 2.14)	(0.59, 1.27)	(0.6, 1.31)
MAE	(1.01, 1.73)	(0.45, 1.01)	(0.46, 1.06)
CP	(0.61, 0.49)	(0.78, 0.62)	(0.97, 0.78)
AIW	(2.05, 2.9)	(1.32, 2.43)	(2.72, 3.36)

Table A.16: Performance measures for each model by data set (train, test) when Block 3 (out of 16 spatio-temporal blocks) is left out as test set.

Block 4		Models	
Measure	INLA	INLA-RF1.1	INLA-RF1.2
RMSE	(1.39, 1.96)	(0.61, 1.56)	(0.62, 1.57)
MAE	(1.03, 1.71)	(0.47, 1.3)	(0.47, 1.33)
CP	(0.60, 0.46)	(0.79, 0.59)	(0.97, 0.76)
AIW	(2.04, 3.14)	(1.32, 2.67)	(2.78, 3.58)

Table A.17: Performance measures for each model by data set (train, test) when Block 4 (out of 16 spatio-temporal blocks) is left out as test set.

Block 5		Models	
Measure	INLA	INLA-RF1.1	INLA-RF1.2
RMSE	(1.36, 1.83)	(0.59, 1.19)	(0.60, 1.19)
MAE	(1.00, 1.32)	(0.44, 0.92)	(0.45, 0.94)
CP	(0.63, 0.62)	(0.79, 0.69)	(0.97, 0.82)
AIW	(2.09, 2.74)	(1.34, 2.3)	(2.71, 3.25)

Table A.18: Performance measures for each model by data set (train, test) when Block 5 (out of 16 spatio-temporal blocks) is left out as test set.

Block 6		Models	
Measure	INLA	INLA-RF1.1	INLA-RF1.2
RMSE	(1.37, 1.32)	(0.61, 0.76)	(0.61, 0.75)
MAE	(1.02, 1.02)	(0.46, 0.64)	(0.46, 0.64)
CP	(0.65, 0.74)	(0.79, 0.87)	(0.97, 1)
AIW	(2.17, 2.76)	(1.37, 2.19)	(2.76, 3.25)

Table A.19: Performance measures for each model by data set (train, test) when Block 6 (out of 16 spatio-temporal blocks) is left out as test set.

Block 7		Models	
Measure	INLA	INLA-RF1.1	INLA-RF1.2
RMSE	(1.38, 1.65)	(0.6, 1.11)	(0.61, 1.14)
MAE	(1.02, 1.24)	(0.45, 0.92)	(0.46, 0.96)
CP	(0.62, 0.62)	(0.78, 0.67)	(0.97, 0.94)
AIW	(2.11, 2.61)	(1.34, 2.2)	(2.75, 3.21)

Table A.20: Performance measures for each model by data set (train, test) when Block 7 (out of 16 spatio-temporal blocks) is left out as test set.

Block 8		Models	
Measure	INLA	INLA-RF1.1	INLA-RF1.2
RMSE	(1.36, 1.53)	(0.6, 1.14)	(0.6, 1.07)
MAE	(1.01, 1.03)	(0.45, 0.95)	(0.46, 0.88)
CP	(0.64, 0.85)	(0.78, 0.71)	(0.97, 0.85)
AIW	(2.14, 3.09)	(1.35, 2.63)	(2.72, 3.51)

Table A.21: Performance measures for each model by data set (train, test) when Block 8 (out of 16 spatio-temporal blocks) is left out as test set.

Block 9	Models		
Measure	INLA	INLA-RF1.1	INLA-RF1.2
RMSE	(1.4, 1.18)	(0.59, 1.04)	(0.6, 1.02)
MAE	(1.04, 0.98)	(0.46, 0.78)	(0.46, 0.75)
CP	(0.63, 0.82)	(0.77, 0.78)	(0.97, 0.96)
AIW	(2.14, 2.85)	(1.33, 2.31)	(2.69, 3.27)

Table A.22: Performance measures for each model by data set (train, test) when Block 9 (out of 16 spatio-temporal blocks) is left out as test set.

Block 10	Models		
Measure	INLA	INLA-RF1.1	INLA-RF1.2
RMSE	(1.37, 1.29)	(0.6, 0.72)	(0.6, 0.72)
MAE	(1.02, 1.03)	(0.46, 0.57)	(0.46, 0.56)
CP	(0.65, 0.78)	(0.78, 0.85)	(0.98, 0.95)
AIW	(2.17, 2.79)	(1.37, 2.27)	(2.74, 3.29)

Table A.23: Performance measures for each model by data set (train, test) when Block 10 (out of 16 spatio-temporal blocks) is left out as test set.

Block 11	Models		
Measure	INLA	INLA-RF1.1	INLA-RF1.2
RMSE	(1.34, 1.81)	(0.6, 1.24)	(0.59, 1.26)
MAE	(1.00, 1.33)	(0.46, 0.98)	(0.45, 0.99)
CP	(0.64, 0.64)	(0.79, 0.7)	(0.97, 0.8)
AIW	(2.15, 2.99)	(1.34, 2.38)	(2.69, 3.35)

Table A.24: Performance measures for each model by data set (train, test) when Block 11 (out of 16 spatio-temporal blocks) is left out as test set.

Block 12	Models		
Measure	INLA	INLA-RF1.1	INLA-RF1.2
RMSE	(1.37, 1.62)	(0.61, 1.02)	(0.6, 1.01)
MAE	(1.01, 1.34)	(0.46, 0.86)	(0.45, 0.85)
CP	(0.64, 0.58)	(0.78, 0.67)	(0.97, 0.9)
AIW	(2.11, 2.78)	(1.34, 2.28)	(2.73, 3.3)

Table A.25: Performance measures for each model by data set (train, test) when Block 12 (out of 16 spatio-temporal blocks) is left out as test set.

Block 13	Models		
Measure	INLA	INLA-RF1.1	INLA-RF1.2
RMSE	(1.39, 1.61)	(0.61, 1.05)	(0.61, 1.09)
MAE	(1.03, 1.17)	(0.46, 0.83)	(0.46, 0.86)
CP	(0.62, 0.78)	(0.77, 0.83)	(0.96, 0.92)
AIW	(2.05, 3.28)	(1.32, 2.71)	(2.75, 3.63)

Table A.26: Performance measures for each model by data set (train, test) when Block 13 (out of 16 spatio-temporal blocks) is left out as test set.

Block 14	Models		
Measure	INLA	INLA-RF1.1	INLA-RF1.2
RMSE	(1.40, 1.2)	(0.61, 0.75)	(0.61, 0.74)
MAE	(1.03, 0.98)	(0.46, 0.60)	(0.46, 0.59)
CP	(0.63, 0.78)	(0.79, 0.88)	(0.97, 0.97)
AIW	(2.16, 3.01)	(1.38, 2.46)	(2.78, 3.42)

Table A.27: Performance measures for each model by data set (train, test) when Block 14 (out of 16 spatio-temporal blocks) is left out as test set.

Block 15		Models	
Measure	INLA	INLA-RF1.1	INLA-RF1.2
RMSE	(1.35, 2.09)	(0.61, 1.26)	(0.61, 1.26)
MAE	(1.00, 1.47)	(0.47, 0.90)	(0.47, 0.90)
CP	(0.64, 0.62)	(0.79, 0.78)	(0.97, 0.86)
AIW	(2.12, 3.11)	(1.38, 2.61)	(2.78, 3.54)

Table A.28: Performance measures for each model by data set (train, test) when Block 15 (out of 16 spatio-temporal blocks) is left out as test set.

Block 16		Models	
Measure	INLA	INLA-RF1.1	INLA-RF1.2
RMSE	(1.35, 2.26)	(0.6, 1.39)	(0.61, 1.40)
MAE	(1.01, 1.66)	(0.46, 1.09)	(0.46, 1.09)
CP	(0.63, 0.56)	(0.77, 0.73)	(0.97, 0.87)
AIW	(2.05, 3.05)	(1.36, 2.68)	(2.76, 3.56)

Table A.29: Performance measures for each model by data set (train, test) when Block 16 (out of 16 spatio-temporal blocks) is left out as test set.

Mean		Models	
Measure	INLA	INLA-RF1.1	INLA-RF1.2
RMSE	(1.83, 2.26)	(0.80, 1.47)	(0.81, 1.47)
MAE	(1.36, 1.75)	(0.61, 1.17)	(0.61, 1.17)
CP	(0.84, 0.88)	(1.04, 0.99)	(1.29, 1.18)
AIW	(2.80, 3.93)	(1.80, 3.27)	(3.66, 4.54)

Table A.30: Performance measures for each model by data set (train, test) across the 16 spatio-temporal blocks.

Appendix B. Predictive performance metrics

We define here the predictive performance metrics used to compare models. We denote by y_i the observed value and by \hat{y}_i the corresponding prediction.

1. *Root mean square error (RMSE)* - a measure of the average magnitude of prediction error, giving higher weight to larger errors:

$$RMSE = \sqrt{\frac{1}{n} \sum_{i=1}^n (y_i - \hat{y}_i)^2}.$$

2. *Mean square error (MAE)* - the average of the absolute differences between predicted and observed values:

$$MAE = \frac{1}{n} \sum_{i=1}^n |y_i - \hat{y}_i|.$$

3. *Coverage probability (CP)* - the proportion of observed values that fall within the predictive interval defined by the 0.025 and 0.975 quantiles (i.e., the 95% credible interval). It assesses the calibration of uncertainty estimates and is defined as

$$CP = \frac{1}{n} \sum_{i=1}^n \mathbb{I} \left(F_{\hat{y}_i}^{-1}(p_l) \leq y_i \leq F_{\hat{y}_i}^{-1}(p_u) \right),$$

where $\mathbb{I}(\cdot)$ is the indicator function, which is 1 if the condition is true and 0 otherwise, $F_{\hat{y}_i}^{-1}(\cdot)$ is the quantile function of the posterior predictive distribution of \hat{y}_i , and p_l and p_u are the lower and upper quantile probabilities (using 0.025 and 0.975, respectively).

4. *Average interval width (AIW)* - the average width of the the 95% credible interval. It reflects the overall uncertainty in the predictions, with narrower intervals indicating higher precision. It is given by

$$AIW = \frac{1}{n} \sum_{i=1}^n \left(F_{\hat{y}_i}^{-1}(p_u) - F_{\hat{y}_i}^{-1}(p_l) \right).$$